TWELFTH EUROPEAN ROTORCRAFT FORUM

Paper No. 18

OVERVIEW OF HELICOPTER WAKE AND AIRLOADS TECHNOLOGY

A. J. Landgrebe

United Technologies Research Center

East Hartford, Connecticut, U.S.A.

September 22 - 25, 1986

Garmisch-Partenkirchen
Federal Republic of Germany

This paper was originally presented at the
American Helicopter Society/Nanjing Aeronautical Institute
International Seminar - "The Theoretical Basis of Helicopter
Technology", Nanjing, China, November 1985.

Deutsche Gesellschaft für Luft- und Raumfahrt e. v. (DGLR)
Godesberger Allee 70, D-5300 Bonn 2, F.R.G.

OVERVIEW OF HELICOPTER WAKE AND AIRLOADS TECHNOLOGY

Anton J. Landgrebe

Manager, Aeromechanics Research
United Technologies Research Center
East Hartford, Connecticut

Abstract

An overview of helicopter aerodynamics technology is presented with emphasis on rotor wake and airloads methodology developed at the United Technologies Research Center (UTRC). The evolution over the past twenty years of various levels of computerized wake geometry models at UTRC, such as undistorted wake, prescribed empirical wake, predicted distorted wake, and generalized wake models for the hover and forward flight regimes, is reviewed. The requirement for accurate wake modeling for flow field and airload prediction is demonstrated by comparisons of theoretical and experimental results. These results include blade pressure distributions predicted from a recently developed procedure for including the rotor wake influence in a full potential flow analysis. Predictions of the interactional aerodynamics of various helicopter components (rotor, fuselage, and tail) are also presented. It is concluded that, with advanced computers and the rapidly progressing computational aerodynamics technology, significant progress is being made toward reliable prediction of helicopter airloads.

Introduction

The task of predicting the flow field and airloads of a helicopter rotor continues to be of primary importance for providing and evaluating improved rotor designs. Also, the capability to predict rotor induced flow velocities away from the main rotor is important for the calculation of aerodynamic interference effects at the fuselage, tail rotor, and tail surfaces. Technological advancement of rotor induced velocity and airloads methodology has focused on the analytical modeling of the rotor wake and the application of higher level computational aerodynamics techniques to represent the blades and their influence on the airflow. This has become possible with the advent of high-speed, large memory computers.

As part of a long-term effort to advance the technology associated with the aerodynamic and aeroelastic behavior of helicopter rotors, studies have been conducted at the United Technologies Research Center (UTRC) to investigate the influence of the rotor wake and develop methodology for predicting the rotor flow field and blade airloads. Publications that document these studies, which span a period of twenty years, are listed in the References (1-24). The scope of this effort has included analytical and experimental research programs, distorted and undistorted wake analyses, single and dual rotor configurations, hover and forward flight conditions, and blade airloads methods ranging from lifting line to full potential. Aerodynamic methods pertaining to these areas, developed at the United Technologies Corporation, are presented herein. Examples of related methodology, developed by other researchers, are indicated within the References and contained in the recent summary papers by Gessow (Ref. 25) and Philippe et al (Ref. 26).

Rotorcraft Wake Analysis

Several methods have been consolidated and expanded to form the Rotorcraft Wake Analysis, a comprehensive helicopter aerodynamic analysis to predict induced flow velocities both at and off the rotor. This computerized analysis, described in Refs. 1 and 2, is normally used in conjunction with rotor performance and airloads analyses. Descriptions and applications of earlier computer analyses which helped form the component and auxiliary programs of the Rotorcraft Wake Analysis can be found in the References. These include the following analyses:

- UTRC Prescribed Wake Hover Performance Analysis (Refs. 4,5).
- UTRC Prescribed Wake Rotor Inflow and Flow Field Prediction Analysis (Refs. 13, 23).
- UTRC Rotor Wake Geometry Analysis (Ref. 3).
- UTRC Rotor Induced Empennage Vibratory Airloads Analysis (RIEVA, Ref. 20).
- UTRC Rotor/Wing Aerodynamic Interaction Analysis (Ref. 24).
- Sikorsky Wing and Body Aerodynamic Techniques Analysis (WABAT, Ref. 32).
- Sikorsky Circulation Coupled Helicopter Aerodynamic Performance Analysis (CCHAP, Refs. 10, 27).

A schematic of the Rotorcraft Wake Analysis showing the input, output, and capabilities of the computer program is presented in Fig. 1. For forward flight, the blade controls and response information are obtained from a separate blade airload and response analysis, as shown in Fig. 1, or test data. For hover, the operating conditions are normally input directly and rotor airloads and performance calculations are self-contained in the computer program. As shown in Fig. 1, the capabilities of the Rotorcraft Wake Analysis and auxiliary programs include hover and forward flight conditions; single rotor, dual rotor, and tail rotor configurations; and wing, fuselage, and tail surface components. Refinement of the fuselage and tail rotor capabilities are currently in progress.

Briefly, the fundamental technical approach for the Rotorcraft Wake Analysis consists of the representation of each blade by a segmented lifting line, and the wake of the rotor by discrete segmented vortex filaments consisting of trailing vorticity, which result from the spanwise variation of blade bound circulation. The distribution of blade and wake circulation changes with azimuth position and is assumed periodic for each rotor revolution. The blades are divided into a finite number of radial segments, and the induced velocity at the center of each selected blade segment is computed by summing the contributions of all bound and trailing wake segments. The contribution of each vortex segment is obtained through use of the Biot-Savart law, which expresses the induced velocity in terms of the circulation strength of the vortex segment and its geometric position relative to the blade segment at which the induced velocity is

desired. The blade bound circulation distribution is determined at each blade azimuth by expressing the wake circulations and induced velocities in terms of the unknown bound vortex strengths by means of the Biot-Savart law, and developing a set of simultaneous equations relating the bound circulation and local blade angle of attack at each blade segment. These equations thus involve the known flight condition, wake geometry, two-dimensional airfoil data, blade motion and control parameters, and the unknown blade bound circulation values. Solution of these equations yields the desired blade bound circulation values, which, when combined with the appropriate geometric relations in the Biot-Savart law, produce the required induced velocities at or away from the rotor blades. The influence of realistic airfoil data and blade motions and controls (e.g., for rotor trim) can be included through an iterative coupling with a blade airloads and performance program. The influence of the shed vorticity behind a blade, due to the time variation of blade bound circulation, can be included by the use of unsteady two-dimensional airfoil data in the airloads program.

Rotor Wake Geometry

Generality regarding the specification of the rotor wake geometry was retained in the computer program. This was accomplished by requiring only that the coordinates of the wake segment end points be stored for computational purposes in a prescribed format with various options for obtaining the coordinates. This facilitates the adaptation of improved wake models to the program as they become available. The wake geometry representation is either generated internally in the computer program, prescribed by input, or generated by a separate wake geometry program. At the present time, the following options are available:

1) A classical wake model is available for hover and forward flight, for which the wake coordinates are computed internally. This is the classical representation of the wake from each blade by skewed, helical vortex filaments simulating an undistorted sheet of vorticity defined geometrically by flight condition and momentum considerations.

2) An undistorted wake model with tip vortex roll-up is available for hover and forward flight, for which the undistorted wake coordinates are computed internally. For the undistorted wake representation, wake distortions are neglected, but the roll-up of the outer vortex filaments into a concentrated tip vortex can be modeled by combining the outer filaments into a tip vortex filament at a prescribed azimuthal distance from the blade.

3) Distorted wake geometries (experimental or analytical) may be prescribed in coordinate form. If analytical, the UTRC Rotor Wake Geometry Analysis, Ref. 3, is currently used to generate the tip vortex coordinates.

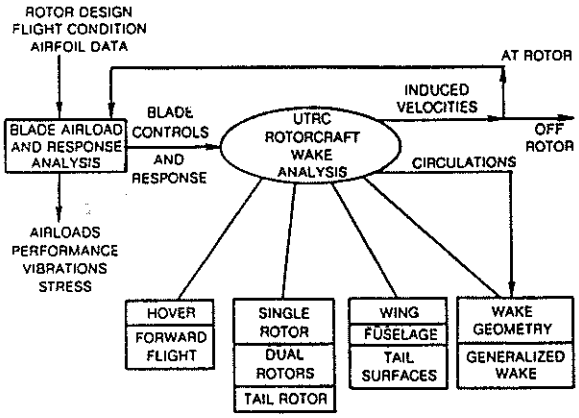

Fig. 1 Schematic of Rotorcraft Wake Analysis Showing Input/Output and Capabilities

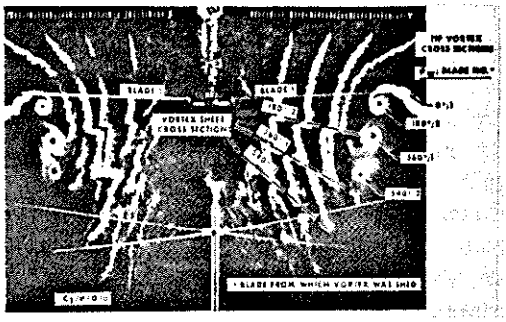

Fig. 3 Flow Visualization Photograph of Cross Section of Hovering Rotor Wake

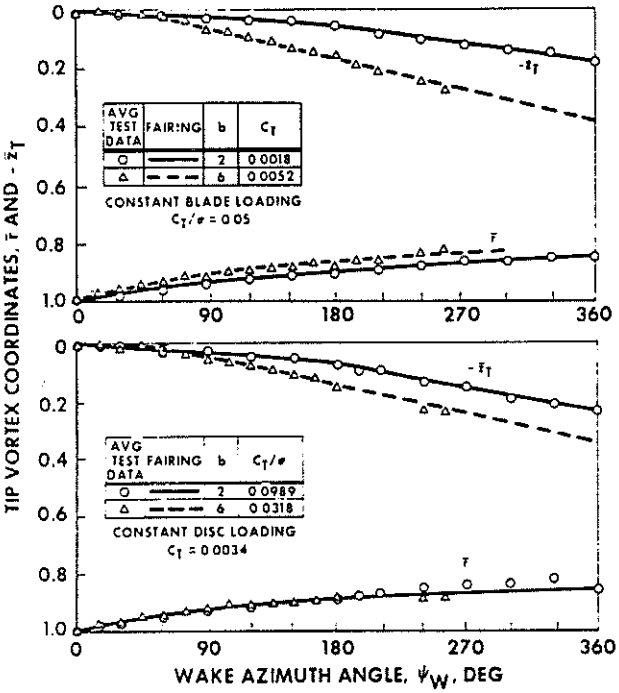

Fig. 4 Tip Vortex Coordinates of Hovering Rotor Showing Effect of Number of Blades and Thrust Level

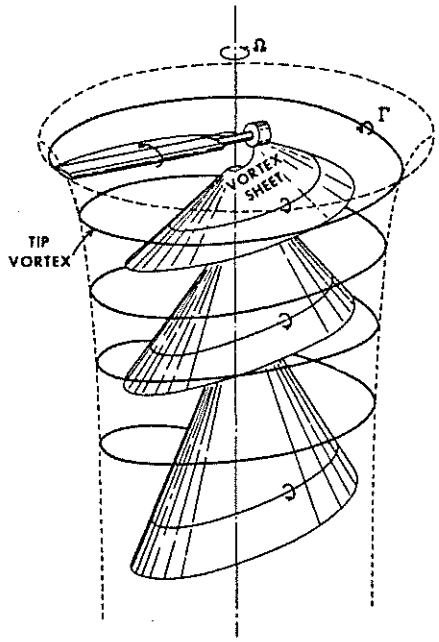

Fig. 2 Hovering Rotor Wake Structure

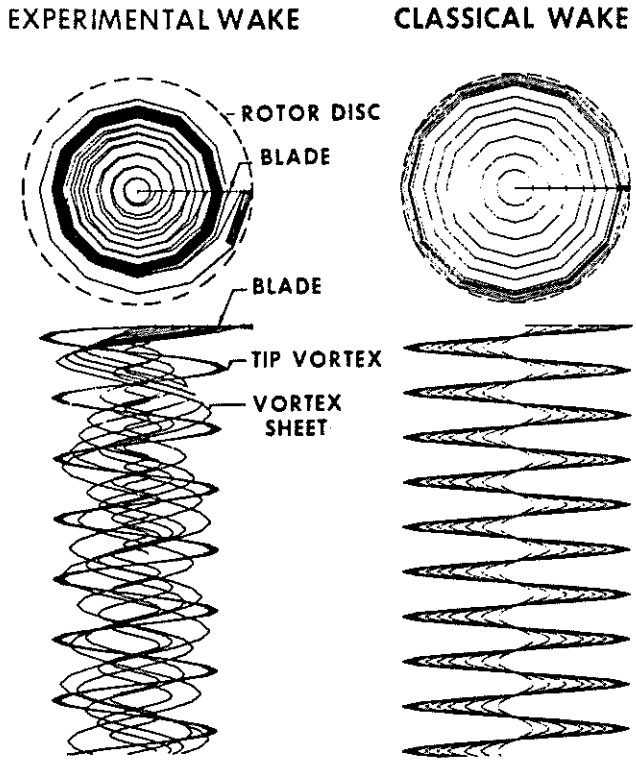

Fig. 5 Computer Wake Representations for One Blade of a Hovering Rotor

4) A generalized wake model is available which is based on generalized experimental wake equations (Refs. 4, 5) for hover and generalized analytical wake equations (Refs. 14, 16) for forward flight.

A computerized method for predicting rotor wake geometry is the UTRC Wake Geometry Analysis (Refs. 3,4). The computation of the wake geometry is initiated by specifying an initial blade circulation distribution, related wake circulation strengths, and an initial wake geometry (normally undistorted wake). The classical Biot-Savart law is applied to compute the velocities induced by each blade and wake vortex segment at the end points of all wake vortex segments. These velocities are then integrated over a small increment in time to define a new wake geometry. The process is continued until a converged wake geometry corresponding to the initial estimate of the blade bound circulation is obtained. A new distribution of blade bound circulation is then computed using the calculated wake geometry in a rotor airloads and response analysis, and the steps are repeated to iterate to a compatible wake geometry-circulation solution. Vortex core models are included for close blade-vortex passage.

Hover Wake Geometry

For hovering rotor wake geometry, the fundamental wake structure depicted in Fig. 2 was confirmed in the 1960's and early 1970's during model rotor tests of rotors with varying numbers of blades, twist, taper, camber, tip design, thrust level, tip speed, blade radial length, and blade vertical and azimuthal spacing (Refs. 4-8). Smoke flow visualization was used to photograph cross sections of the wake as shown in the sample flow visualization photograph in Fig. 3. The blade azimuth travel relative to the wake cross sections (ψ_w, wake age) is indicated on Fig. 3.

The wake contains two primary components. The first, and most prominent, is the strong tip vortex which arises from the rapid rolling up of the portion of the vortex sheet shed from the tip region of the blade. The second feature is the vortex sheet shed from the inboard portion of the blade. The vertical or axial transport velocity near the outer end of the inboard vortex sheet is much greater than that of the tip vortex. The vertical velocity of the vortex sheet also increases with radial position, resulting in a substantially linear cross section of the vortex sheet at any specific azimuth position. These characteristics largely result from the velocities induced by the strong tip vortex. Although the radial extent of the vortex sheet is depicted in Fig. 2 as ending abruptly, it probably retains some connection with the tip vortex. The exact nature of this connection, however, has been difficult to distinguish in flow visualization studies. Flow visualization photographic data were analyzed to determine wake coordinates for the various rotor design and operating condition parameters. Sample tip vortex coordinate plots are presented in Fig. 4 which shows the effect of the number of blades and thrust level. Generalized wake equations were developed for the tip vortex and inboard wake (vortex sheet) geometry, as generalized functions of number of blades, twist, and thrust level (Refs. 4 and 5). The generalized wake geometry equations are used in the UTRC Prescribed Wake Hover Performance Analysis (hover analysis component of Rotorcraft Wake Analysis) to define the wake geometry. A sample computerized wake representation for one blade of a hovering rotor is shown in Fig. 5. An experimental wake representation

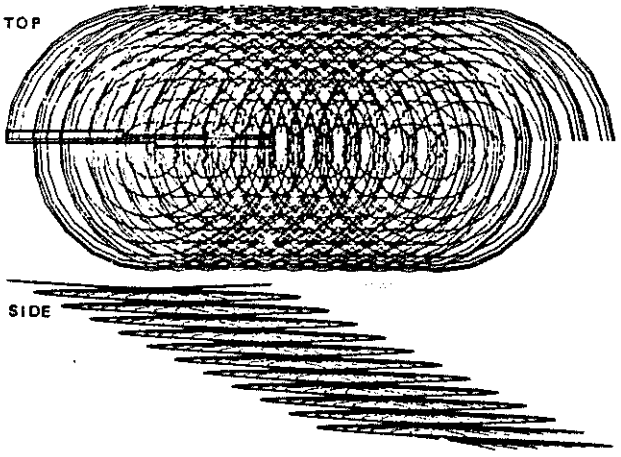

Fig. 6 Classical Undeformed Wake Representation for a 30 Kt Forward Flight Condition

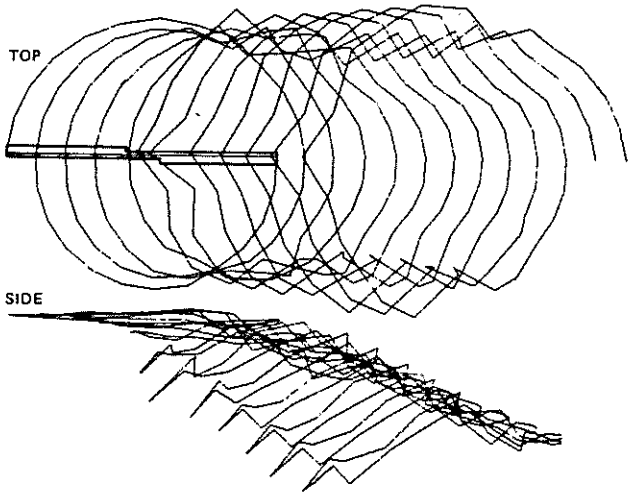

Fig. 7 Distorted Tip Vortex Representation for a 30 Kt Forward Flight Condition

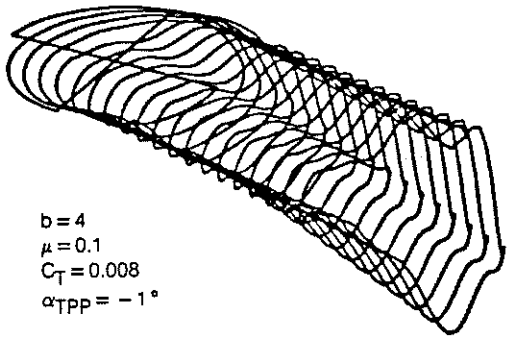

Fig. 8 Isometric View of Generalized Distorted Tip Vortices

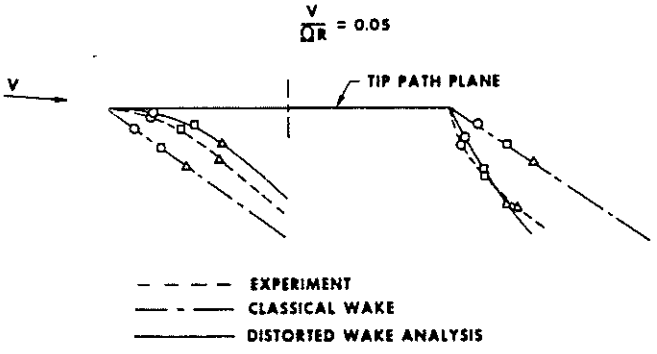

Fig. 10 Comparison of Theoretical and Experimental Fore and Aft Wake Boundaries

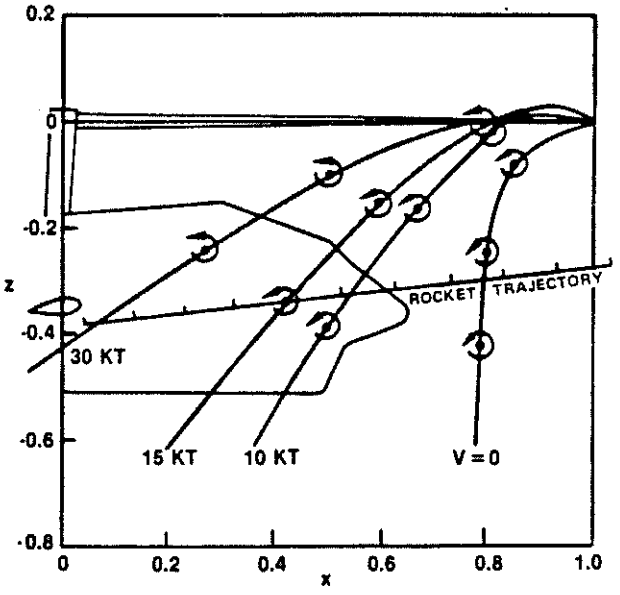

Fig. 9 Experimental Rotor Wake Boundaries and Tip Vortex Locations for Hover and Low Speed Flight

based on the generalized wake equations is presented along with a classical wake representation.

The Wake Geometry Analysis has successfully predicted the trends in hover wake geometry with variations of rotor design and operating parameters. The capability of the analysis to predict changes in tip vortex geometry with variations in thrust level, number of blades, blade twist, aspect ratio, and tip speed has been demonstrated (Refs. 4,5, and 9). The general wake features predicted by the analysis were found to be in good agreement. This includes the ability of the analysis to predict the decrease in tip vortex stability as the distance from the rotor disk is increased. The quantitative accuracy of the analysis is limited by one major shortcoming; namely, the inability to predict the vertical transport velocity of the tip vortex with sufficient accuracy to determine the tip vortex passage distance beneath the following blade. Calculations of rotor airloads and performance are very sensitive to this distance. This problem was largely resolved in a significant extension of the Prescribed Wake Hover Performance Analysis to the Sikorsky Circulation Coupled Hover Analysis Program (CCHAP) (Refs. 10 and 28). CCHAP provides wake geometry refinements which are based on the blade loading solution. The technique applies to both conventional rotor geometries and the more general case where planform or nonlinear twist variations previously restricted the use of the Prescribed Wake Program due to the lack of appropriate experimental wake geometries in the generalized wake data base.

Forward Flight Wake Geometry

Classically, for forward flight, the wake shed from a rotor blade has been modeled as an undistorted skewed helical sheet of vorticity of varying strength, with a skew angle defined by rotor attitude and flight condition. The vortex sheet is approximated with discrete vortex filaments of appropriate strength and radial location. An example of the classical undeformed wake for forward flight (30 kts) is shown in Fig. 6. The tip vortex geometry for 30 kts forward flight, as predicted by the UTRC Wake Geometry Analysis, is shown in Fig. 7. A sample isometric view of tip vortices from a generalized wake model is shown in Fig. 8. A major characteristic of the real wake geometry is the rollup of the outer portion of the vortex sheet into a tip vortex displaced from the undistorted geometry. The characteristic wake distortion features observed from experimental results are present in the predicted tip vortex geometries. The forward and lateral sides of the wake are distorted toward the rotor relative to the undistorted wake model. This results in close blade-vortex passages which can introduce large local azimuthal and spanwise gradients in blade airloads. On the advancing side of the rotor the tip vortices are aligned with the passing blades (especially in the rear quadrant) resulting in vibratory excitation and impulsive noise. In low speed forward flight, the tip vortices pass over the rotor disk before they move down, as shown in Fig. 9, which is based on smoke flow visualization (Refs. 11 and 12). This feature is predicted by the Wake Geometry Analysis (Fig. 7). Experimental wake geometry data for forward flight conditions are limited, but comparisons of Wake Geometry Analysis results with available data are presented in Figs. 10 and 11. Figure 10 from Ref. 3 shows a comparison of the classical, experimental, and predicted wake boundaries. Figure 11 from Ref. 13 illustrates comparisons of the experimental (water tunnel), undistorted, and calculated distorted tip vortex displacements from the rotor disk as a function of wake age for two different advance ratios and blade azimuth angles.

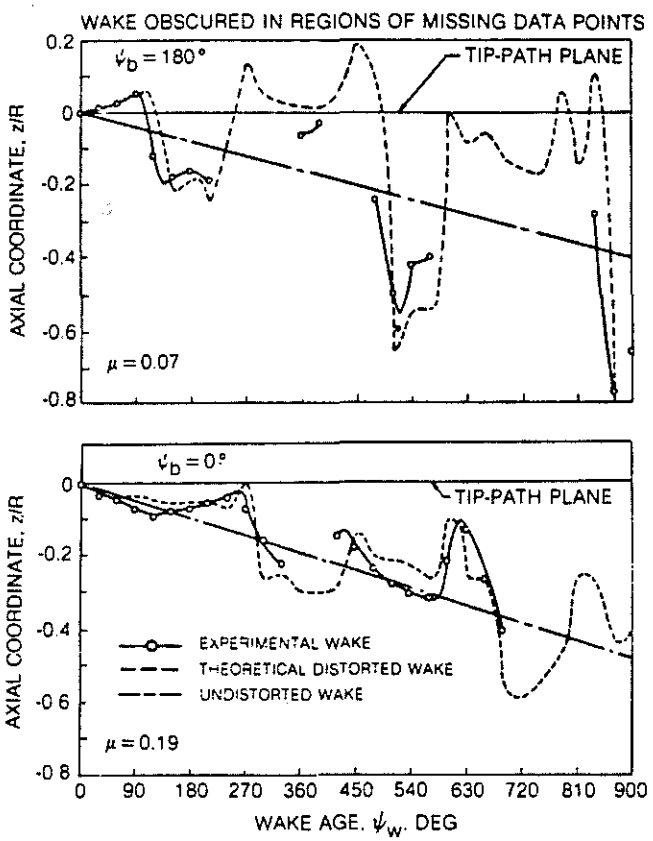

Fig. 11 Comparison of Theoretical and Experimental Tip Vortex Coordinates (Normal to Rotor Disk)

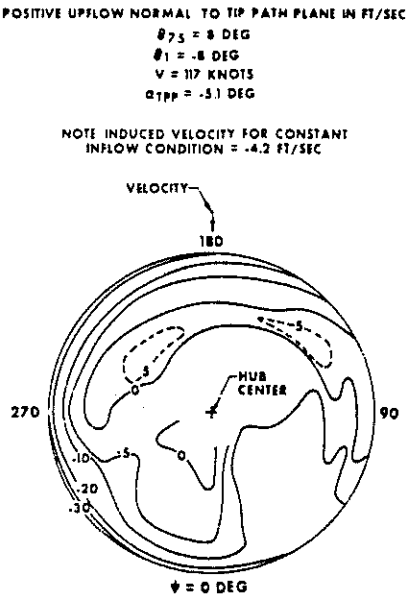

Fig. 13 Predicted Blade Induced Velocity Variation Based on Distorted Wake Geometry

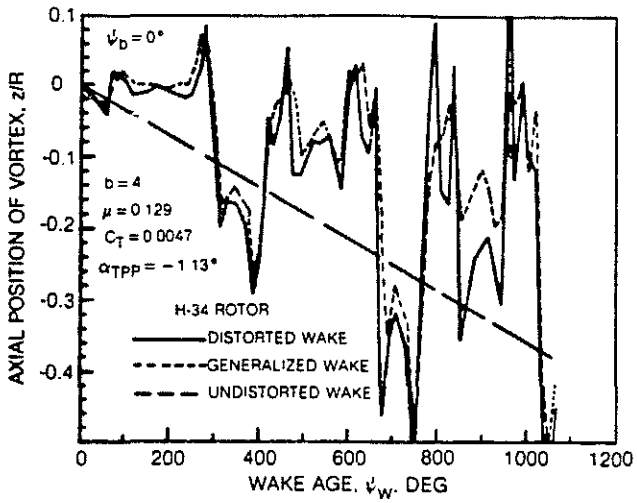

Fig. 12 Comparison of H-34 Predicted Distorted, Undistorted, and Generalized Wake Geometries (Normal to Rotor Disk)

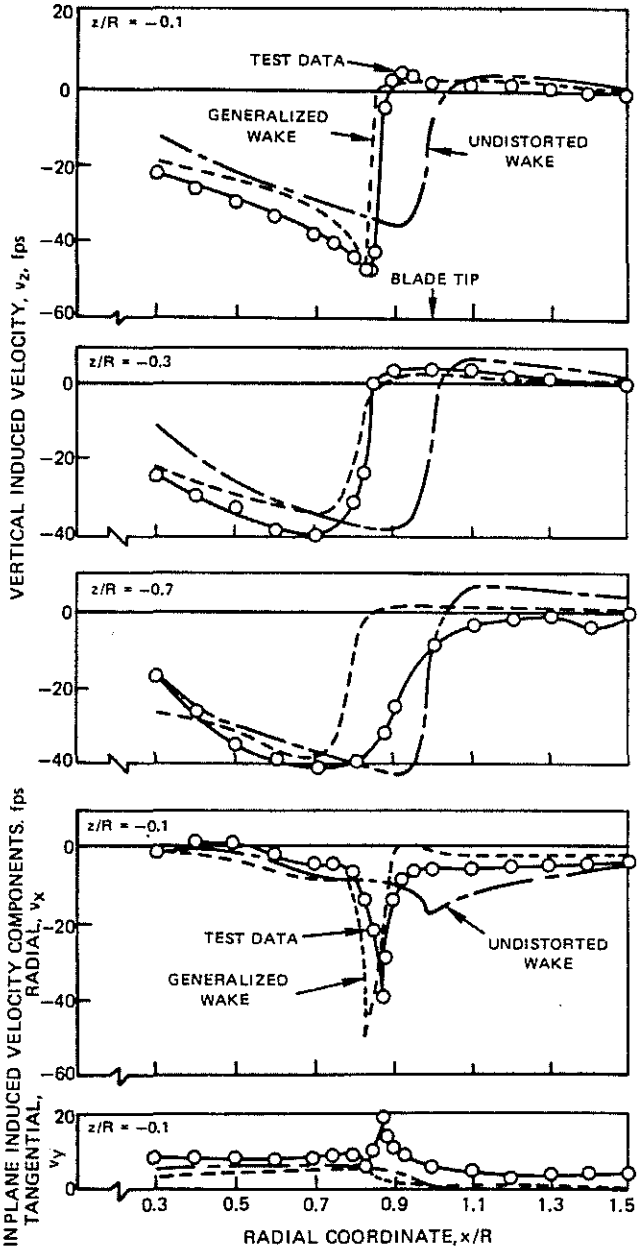

Fig. 14 Predicted vs. Measured Instantaneous Induced Velocity Components of a Full-Scale Hovering Rotor

A more recent investigation of helicopter rotor wake geometry and its influence in forward flight is reported in Refs. 14 and 15 and summarized in Ref. 16. This analytical investigation was conducted to generalize the wake geometry of a helicopter rotor in forward flight and to demonstrate the influence of including wake deformation in the prediction of rotor airloads and performance. Predicted distortions of the tip vortex of each blade relative to the classical undeformed geometry were generalized for vortex age, blade azimuth, advance ratio, thrust coefficient, rotor disk attitude, and number of blades based on a representative blade design. The equations for the wake geometry generalization for forward flight are documented in Refs. 14 and 16. A computer module and charts (Ref. 15) were developed for approximating wake geometry and identifying wake boundaries and locations of blade-vortex passage. Various views of the tip vortex patterns for variations of the above parameters are included in Ref. 15. A sample generalized wake isometric view is shown in Fig. 8. Figure 12 shows an example of the capability of the generalized wake model to represent the predicted H-34 axial tip vortex geometry (normal to the rotor disk). The general agreement between the two wake models is encouraging, considering that the generalization is thus far based on representative blade design parameters. Near the rotor, the axial tip vortex distortions are generally significantly greater than the lateral and longitudinal distortions.

The tip vortex distortions relative to the undistorted wake geometry are most sensitive to advance ratio and are insensitive to disk attitude. The amplitude of the tip vortex distortions is proportional to thrust coefficient, but the characteristic shape of the principal distortions is insensitive to thrust coefficient. The tip vortex geometry was found to be much more sensitive to blade twist than blade aspect ratio. The wake distortions are most complex at low advance ratios (e.g., 0.05) where the difficulty of accurate wake geometry prediction is compounded by the large number of close blade-vortex passages and the movement of the tip vortices above and then down through the rotor disk resulting in blade-vortex impingement (Fig. 9).

Flow Velocities

An example of a predicted variable induced velocity map (induced at the blade during a blade revolution) based on a distorted wake geometry from the Rotor Wake Geometry Analysis is shown in Fig. 13. The highly variable character of the inflow for a 117 kt flight condition is demonstrated. Even greater variations have been predicted, particularly on the advancing side, for other flight speeds and rotor disk attitudes for which the tip vortices are closer to the rotor.

In order to investigate helicopter rotor airflow and demonstrate the accuracy of the Rotorcraft Wake Analysis, correlation studies have been conducted to compare predicted flow velocities with test data from several sources. Reference 1, summarized in Ref. 2, contains theory-test comparisons for ten different test sources and 25 combinations of rotor configuration and test condition. For hover, predicted induced velocities were compared with induced velocity data for a full-scale, two-bladed, OH-13E rotor tested on a test tower at Mississippi State Univ. Three-component velocity measurements were made below the rotor with a split-film total vector anemometer as reported in Ref. 28. Comparisons of measured and predicted instantaneous induced velocity components are

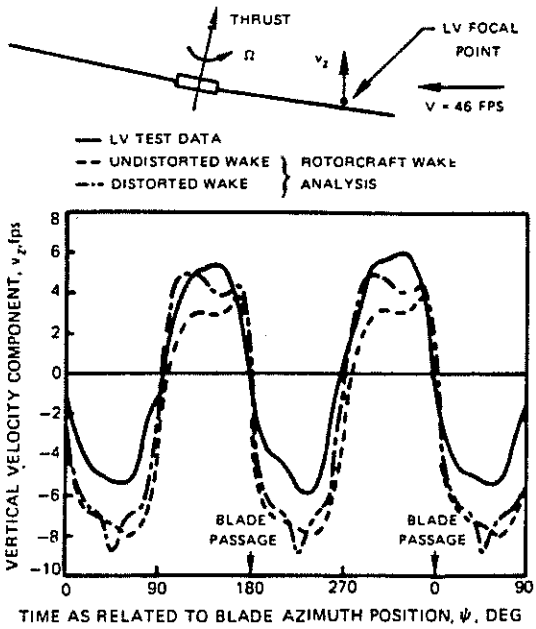

Fig. 15 Predicted vs. Measured Time Variations of the Flow Velocity at a Point Near a UTRC Model Rotor (Advance Ratio = 0.15)

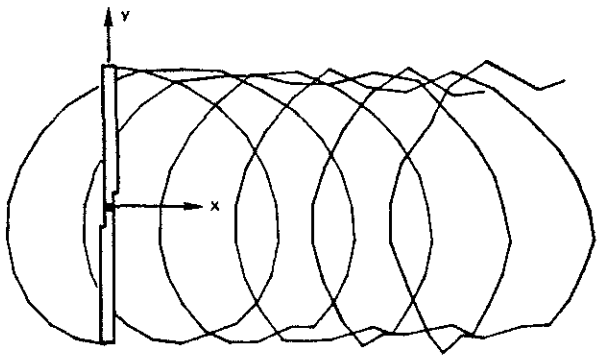

Fig. 16 Predicted Tip Vortex Geometry for NASA Model Rotor (Advance Ratio = 0.18)

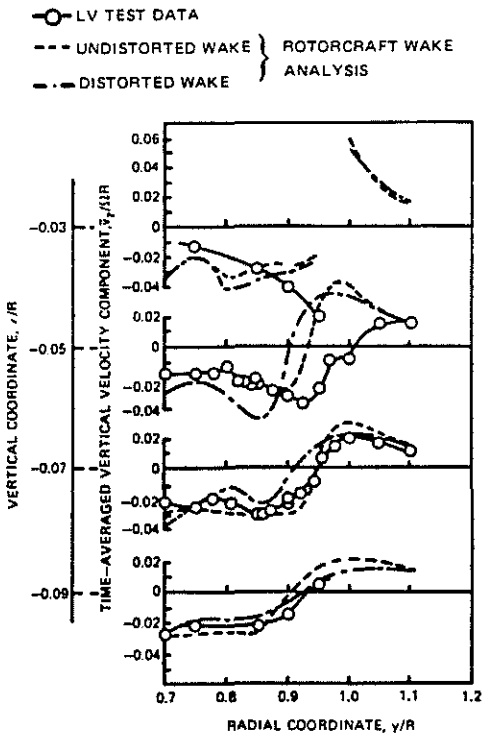

Fig. 17 Predicted vs. Measured Radial Distributions of the Time-Averaged Vertical Velocity Component Beneath the Advancing Side of a NASA Model Rotor (Advance Ratio = 0.18)

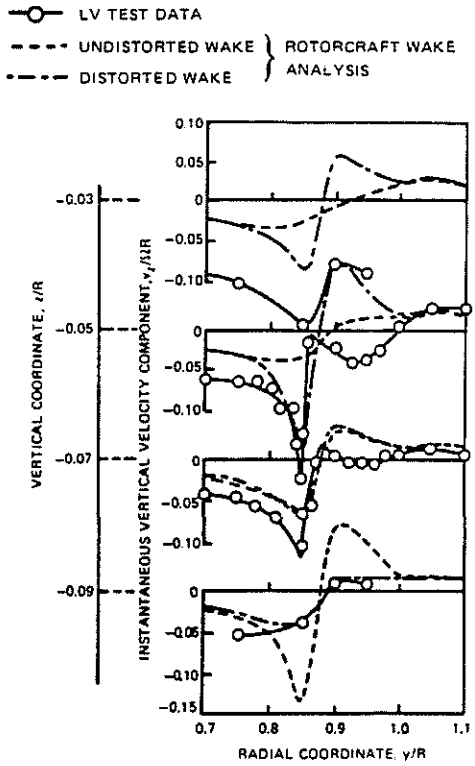

Fig. 18 Predicted vs. Measured Radial Distributions of the Instantaneous Vertical Velocity Component Beneath the Advancing Side of a NASA Model Rotor (Advance Ratio = 0.18)

presented in Fig. 14 for several distances below the rotor and a plane of measurement point 90 degrees behind one of the blades. Predicted induced velocities based on both the generalized wake equations and the undistorted wake representation are presented. Good agreement is indicated near the rotor. At z/R = -0.7, the correlation deteriorates near the wake boundary because no attempt was made in the prescribed generalized wake representation to model the unstable behavior of the far wake which has been evident in smoke and Schlieren flow visualization movies taken at UTRC.

Laser velocimeter (LV) techniques were applied at UTRC to a two-bladed model rotor in a wind tunnel, and flow velocity time-histories were measured at several fixed points in close proximity to the rotor. This demonstration test is described in Ref. 17, and a comparison of predicted vertical and streamwise velocity components with test data at several points are presented in Ref. 1. Velocity data were measured at points above and below the upstream rotor azimuth position (ψ = 180 deg). As reported in Refs. 1 and 2, the Rotorcraft Wake Analysis was used to calculate time histories of the instantaneous velocity components for several of the LV data points. Both an undistorted wake and a distorted wake representation obtained from the UTRC Wake Geometry Analysis were used in the calculations. A sample comparison of the predicted and measured time histories of the vertical velocity component at one point, 0.75R forward of the hub and 0.02R above the passing blade, is presented in Fig. 15. The flow velocity is presented for varying time as related to the azimuth position of one of the two blades, and is shown to be periodic with blade passage interval (two cycles per rotor revolution). The time histories predicted using the Rotorcraft Wake Analysis are shown in Fig. 15 to be generally in good agreement with the time history measured with the laser velocimeter.

A laser velocimeter was also used by Biggers and Orloff at the NASA Ames Research Center to measure flow velocities near a two-bladed model rotor in a wind tunnel. The data reported in Ref. 29, consisting of two components of velocity in the outboard vicinity of the blades at two azimuth positions (ψ = 90 and 270 deg), were used for comparison with the Rotorcraft Wake Analysis predictions as reported in Ref. 1. Time-averaged and instantaneous velocity components in the vertical and streamwise directions were measured near a 7-ft diameter rotor operating at an advance ratio of 0.18.

In order to show the sensitivity of the predicted velocities to tip vortex distortions, the Rotorcraft Wake Analysis was run with both undistorted and distorted wake representations. A top view of the distorted tip vortices predicted by the UTRC Wake Geometry Analysis for the rotor and test condition under consideration is shown in Fig. 16 for the blades in the 90 and 270 deg azimuth positions. The tip vortex crossing the advancing blade was predicted to be at 0.045R below the 0.86R radial location of the rotor, which compares favorably with the measured 0.05R below the 0.85R location. The undistorted tip vortex was calculated to be 0.104R below the 0.87R location.

In Fig. 17, the predicted and experimental radial distributions of the time-averaged vertical velocity component are presented for several elevations beneath the advancing side of the rotor (y-axis). The radial distributions are characterized by downflow inside the wake changing to

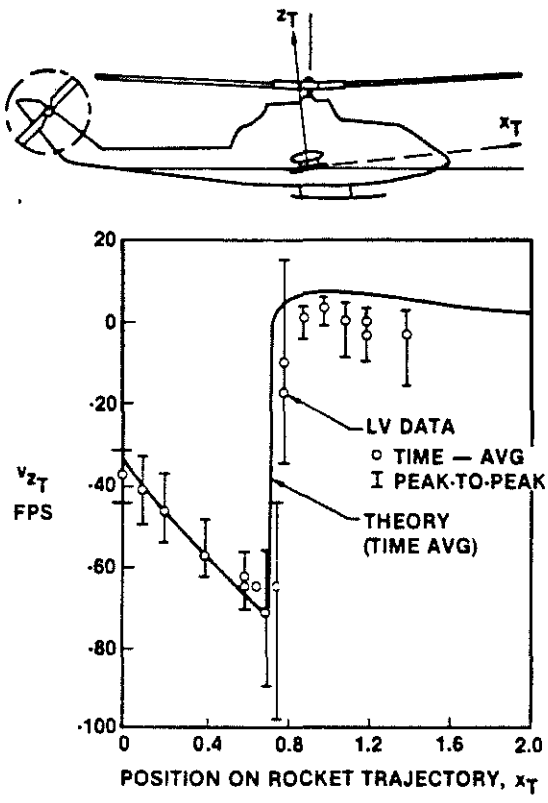

Fig. 19 Comparison of Measured and Predicted Flow Velocities Normal to a Rocket Trajectory for a Hover Condition

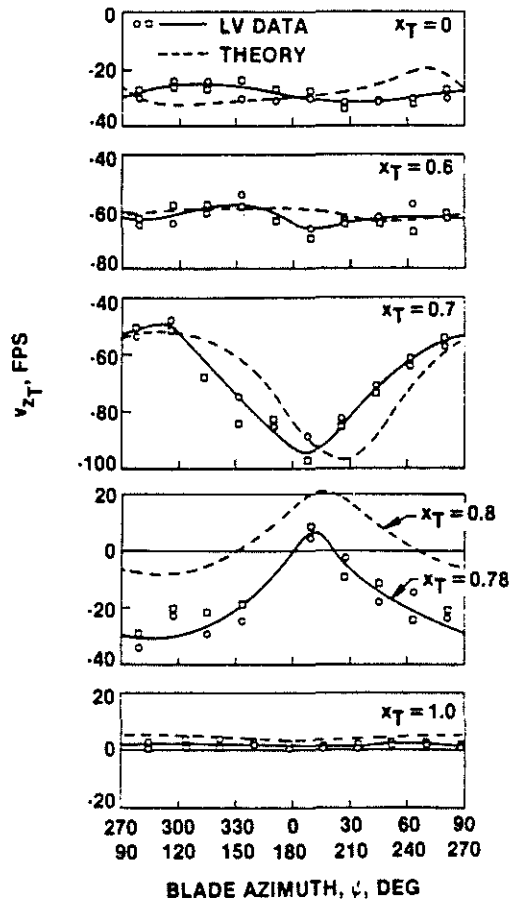

Fig. 20 Comparison of Measured and Predicted Time Variant Flow Velocity Component at Several Points on a Rocket Trajectory for a Hover Condition

upflow outside the wake primarily due to the passage of the tip vortices. The gradients diminish with increasing distance from the rotor and wake boundary. The predicted velocity distributions are in agreement with these features. Radial distributions of instantaneous vertical velocities are presented in Fig. 18 for points along the noted elevations beneath the advancing blade when at ψ = 90 deg (same measurement point locations as in Fig. 17). As mentioned above, the measured tip vortex location was at y/R = 0.85 and z/R = -0.05. This tip vortex location is evident in the measured instantaneous velocity distribution which indicates large gradients in velocity in the vicinity of this point. The presence of the predicted distorted tip vortex is also evident at this location, whereas the undistorted tip vortex is evident at the -0.09 elevation which is attributable to its further distance from the rotor. The predicted instantaneous velocities based on the distorted wake representation are thus improved over the undistorted wake results due to the more accurate positioning of the tip vortex.

A more recent comparison of predicted rotor flow velocities with laser velocimeter data is presented in Ref. 11 and summarized in Ref. 12. Time-averaged and time variant flow velocities were measured with a laser velocimeter at UTRC along the rocket trajectory lines of a model AH-1G Cobra helicopter, and the flow velocity components were compared with theoretical predictions.

The laser velocimeter data for the variation along the rocket trajectory of the principally downward component of flow velocity, v_{z_T}, for the hover condition, are presented in Fig. 19. The time-averaged v_{z_T} velocity component is shown to double in magnitude from the rocket launch position (x_T = 0) to the intersection of the trajectory and wake boundary. The increasing downwash trend over the inner wake portion of the rocket trajectory was anticipated and is consistent with the fact that the rocket launch position under consideration is near the center of the wake in hover (r = 0.22), and the downwash in the hovering wake is known to increase with radial position. Moving from inside to outside the wake boundary, an abrupt change in velocity occurs in both magnitude and direction (downflow to upflow). The upflow is not nearly as severe as the downflow because the contributions of the tip vortices and the inboard vortex sheets are opposing outside of the wake, whereas they are additive just inside the wake boundary. The capability of the theory of Refs. 1 and 5 to predict the time-averaged flow from the LV measurements is shown in Fig. 19.

The flow velocities at each flow field point vary with time even in hover due to the rotation of the blades and the associated passage of the wake elements by the field points. The periodic time variation of the flow velocity at points on the rocket trajectory is indicated in Figs. 19 and 20 by the peak-to-peak limits and the time-history variations with rotor azimuth, respectively.

The time variation of the v_{z_T} flow velocity component, at several points on the rocket trajectory, is presented in Fig. 20. Shown are comparisons of the theoretical predictions, based on the prescribed model rotor wake, with the LV data corresponding to specific rotor azimuth positions. The mean of the instantaneous velocities (mean of the measured velocities of individual seedant particles) is indicated for each 15 degree blade azimuth increment, with different symbols used to distinguish between

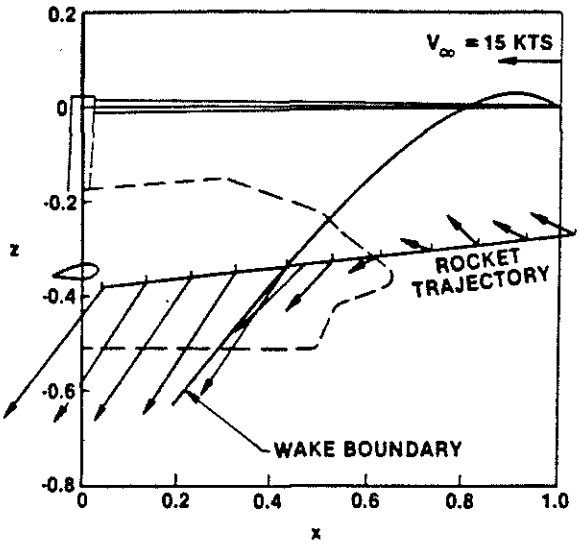

Fig. 21 Measured Time-Averaged Flow Velocities Along a Rocket Trajectory for a 15 Kt Condition

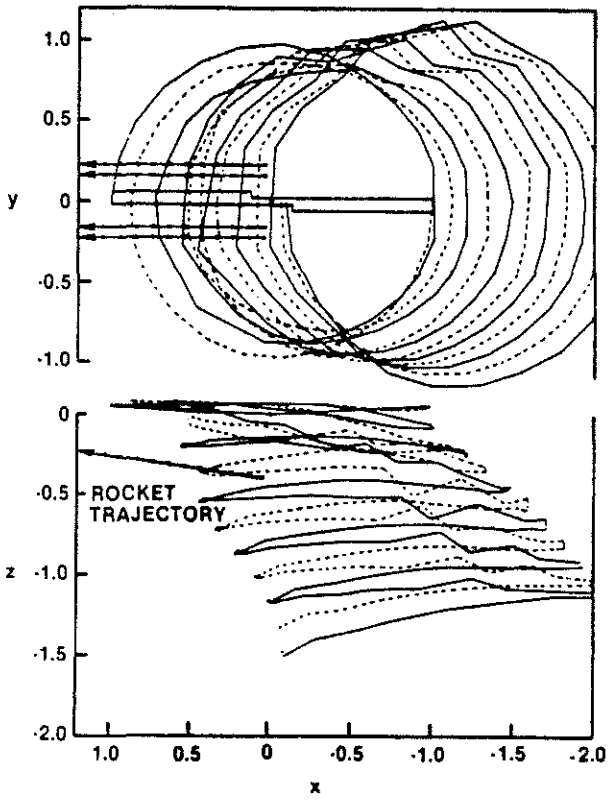

Fig. 22 Predicted Tip Vortex Geometry for 15 Kt Condition

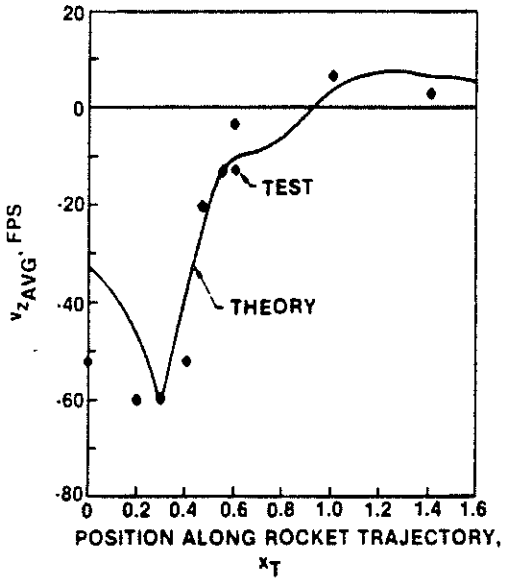

Fig. 23 Comparison of Measured and Predicted Time-Averaged Flow Velocity Normal to a Rocket Trajectory for a 15 Kt Condition

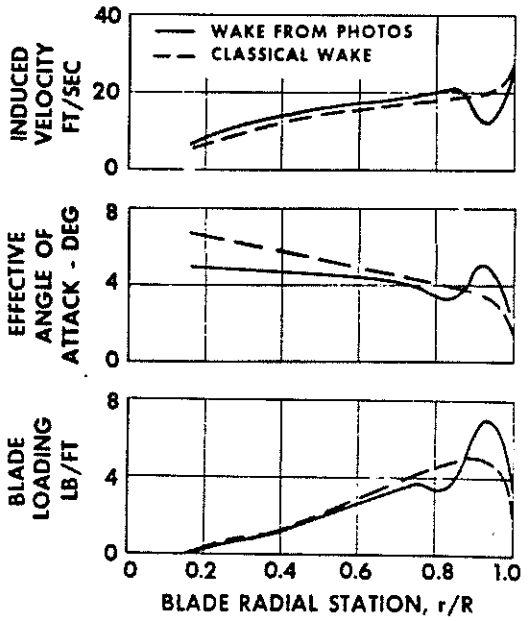

Fig. 24 Predicted Effect of Wake Distortion on Induced Velocity, Angle-of-Attack, and Lift Distributions of a Hovering Rotor Blade

data taken for the first and second half of the rotor revolution. The theory predicts the 2 per rev character and amplification of the peak-to-peak velocity increments near the wake boundary. The significant time variation of the flow velocity component near the wake boundary is mostly due to the periodic passage of the tip vortices past the point on the rocket trajectory. Small geometric increments of the tip vortex produce large velocity phase shifts. This is recognized when it is considered that each one percent vertical displacement of the tip vortex corresponds to a 10 deg phase shift. This indicates the importance of accurately representing the wake if the time variation of the flow velocities at specific points are of interest.

The high sensitivity to wake location is also evident in Fig. 20 in the mean velocity shift between the measured time history at $x_T = 0.78$ and the predicted time history at $x_T = 0.80$. Although the cyclic behavior is in agreement, the shift occurs which is attributable to the extreme gradient of the time-average velocity in the wake boundary region as shown in Fig. 19. It was thus concluded that the analysis is capable of predicting the induced velocity time variation in the flow field for the hover condition. However, the degree of correlation is very dependent on an accurate wake geometry representation.

In Fig. 21, a vector plot of the flow velocities at points on the rocket trajectory for the 15 kt condition is presented which provides a pictorial representation of the influence of the rotor wake. The scaled flow velocities obtained from LV measurements for the isolated rotor are plotted vectorially, with vector lengths in proportion to the 15 kt freestream vector, such that the magnitude and direction of the flow are depicted. The wake boundary from the flow visualization results is also shown. Ahead of the wake boundary, the flow vectors indicate the upflow, the deceleration of the flow, and then the changeover to downflow as the wake boundary is approached. A large increase in flow velocity is observed as the wake boundary is crossed. Although less extreme than for hover, the gradient of the vertical velocity component that occurs near $x_T = 0.4$ was found to be consistent with the wake boundary crossing point on the rocket trajectory determined from the flow visualization results and the predicted wake geometry (Fig. 22).

Predictions of the rotor wake flow velocities, based on the use of the theoretical tip vortex geometry (Fig. 22) with the momentum inboard vortex sheet geometry in the Rotorcraft Wake Analysis, are compared to the test results for the 15 kt isolated rotor condition in Fig. 23. As indicated, the theory correctly predicts the magnitude and gradient of the time-averaged vertical flow velocity component along the trajectory, including the peak downwash value, as the wake boundary is approached from upstream. The difference inside the wake, which also occurred for the horizontal component, is believed to indicate the need for replacing the momentum inboard wake model, used in the Rotorcraft Wake Analysis for the Ref. 11 study, with a more realistic geometry and the need to account for the tip vortex diffusion related to the blade-vortex intersection shown in Fig. 9.

Generally, the results presented above indicate that the Rotorcraft Wake Analysis favorably predicts the features of the velocity distributions in the wake, but the degree of accuracy varies depending on the accuracy of the wake representation. The predicted induced velocities are generally in

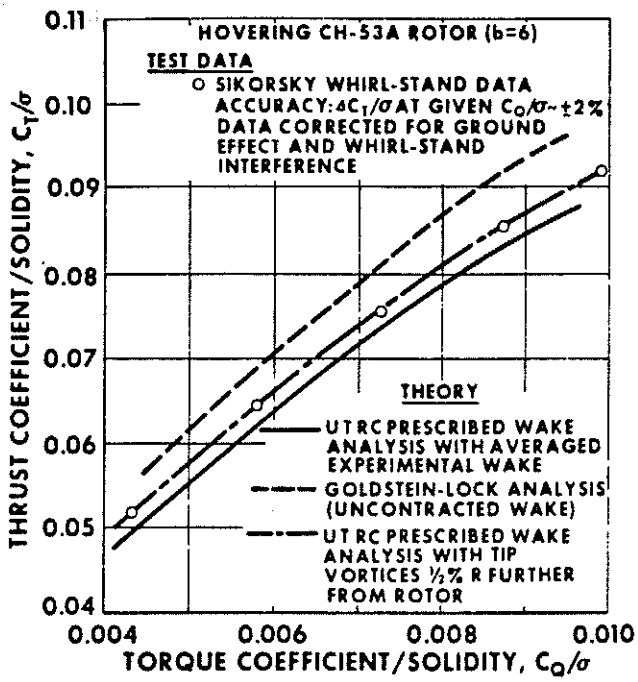

Fig. 25 Effect of Wake Geometry on Predicted Rotor Hover Performance and Comparison With Experiment

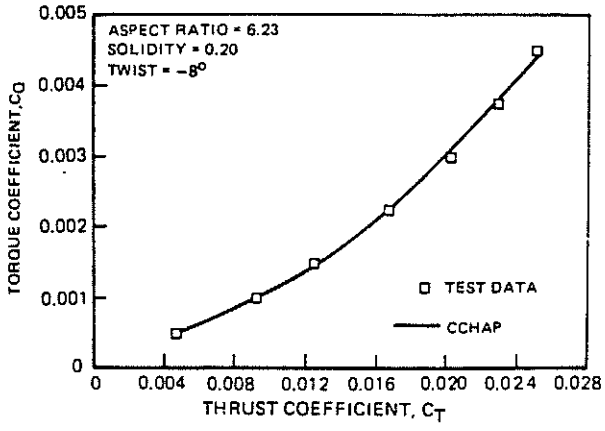

Fig. 27 Improvement of Hover Performance Correlation With a Circulation Coupled Wake for a Low Aspect Ratio Tail Rotor

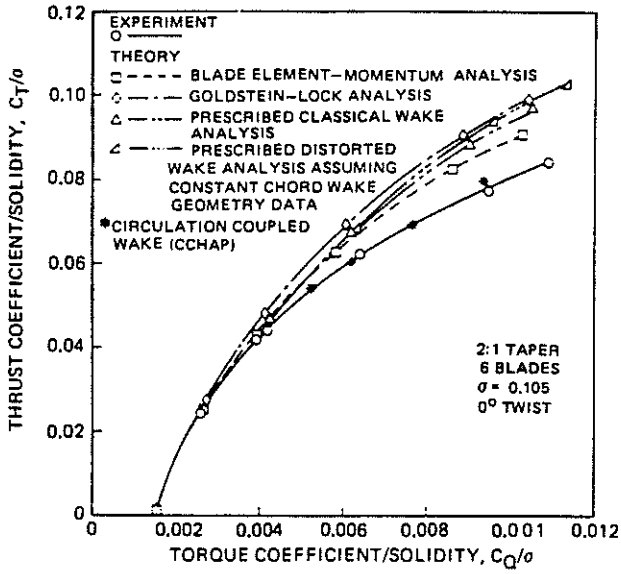

Fig. 26 Improvement of Hover Performance Correlation With Circulation Coupled Wake for a Model Rotor With Tapered Blades

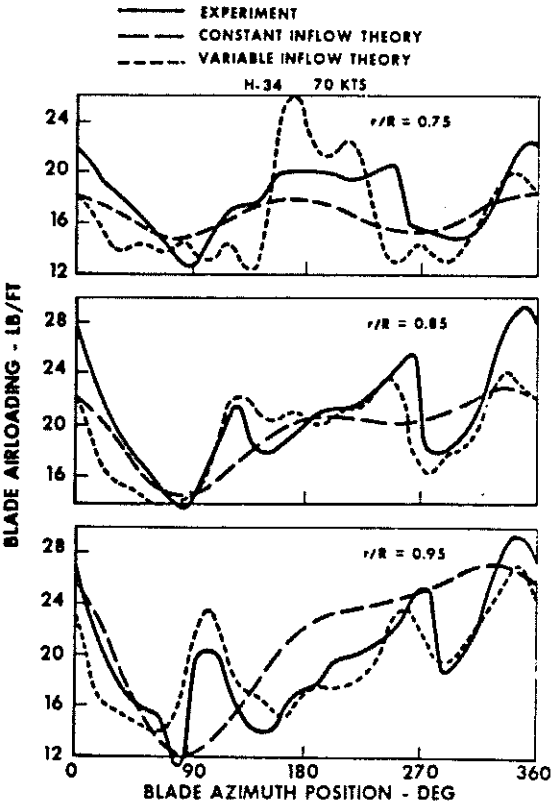

Fig. 28 Comparison of Predicted and Measured H-34 Blade Airload (Lift) Variations

good agreement with measured velocities when a distorted wake representation is used. The successful prediction of characteristic features of both timeaveraged and instantaneous induced velocity distributions in and out of the rotor wake has been demonstrated within the scope of the available test data. However, the degree of accuracy at a specific field point is sensitive to the prescribed wake representation, proximity of the field point to a wake boundary or blade, and the accuracy of the input flight condition, rotor control, and blade motion information.

Blade Airloads

Hover

The importance of properly accounting for wake geometry in the calculation of blade airloads for a hovering rotor was reported in Ref. 6 following the development of the UTRC Prescribed Wake Hover Performance Analysis in the 1960's. A computerized representation of a photographed wake of a model rotor (Fig. 5) was used to calculate and compare the induced velocity, angle of attack, and airload distributions with those based on the classical undistorted wake model as shown in Fig. 24. The influence on the blade airloading, particularly in the outer blade region, was noted. This led to the systematic experimental investigation to generalize hovering rotor wake geometry using flow visualization techniques and to perform a test-theory correlation study for hovering performance (Refs. 4 and 5). The effect of wake geometry on the predicted hover performance of a full-scale, six-bladed CH-53A rotor and comparison with measured performance is shown in Fig. 25. The sensitivity of the rotor performance to tip vortex position in the Prescribed Wake Analysis is also demonstrated. Although the generalized wake geometry was found to provide accurate performance predictions for blade designs within the scope of the available model test data, limitations were found for non-tested designs such as blade taper, nonlinear twist, and low aspect ratio. As mentioned earlier, this was resolved by coupling the blade loading distribution and wake geometry solutions in the Circulation Coupled Hover Analysis Program (CCHAP, Refs. 10, 27). Correlation of CCHAP predicted performance with test data for rotors with tapered and low aspect ratio blades is shown in Figs. 26 and 27.

Forward Flight

The importance of accounting for the rotor wake in the calculation of blade airloads for forward flight conditions was recognized by several researchers in the 1960's. A historical summary of the theoretical airload developments prior to and during that period is presented in Ref. 18. Sample blade airloads from Ref. 3, for which the UTRC Prescribed Wake Analysis was used with a classical wake geometry to predict the variable blade inflow, are compared in Fig. 28 with both experimental airloads and airloads predicted using momentum theory (constant inflow). Although the correlation using the undeformed classical wake was good in some regions, it was found to be unreliable in others. Also, correlation was degraded for flight speeds and operating conditions with more severe close blade-vortex interactions.

The deformation of the forward and lateral sides of the wake toward the rotor disk, shown earlier in Figs. 7 and 8, can result in close blade-vortex passages which can introduce severe local azimuthal and

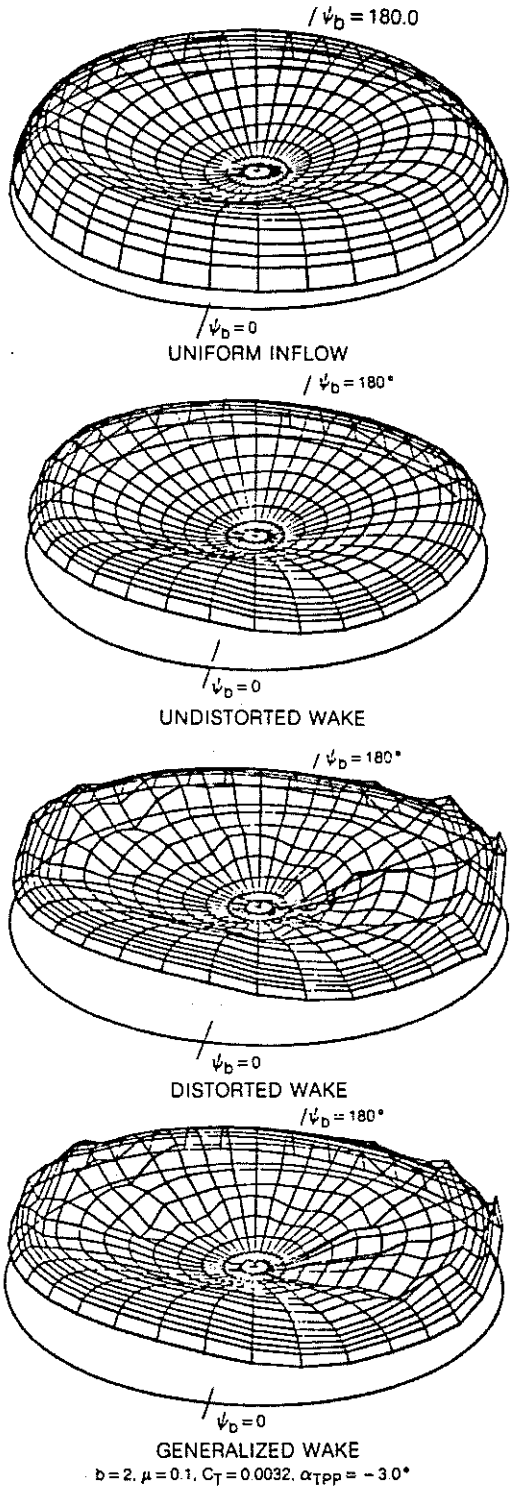

Fig. 29 Blade Lift Distributions Predicted With Various Wake/Inflow Models

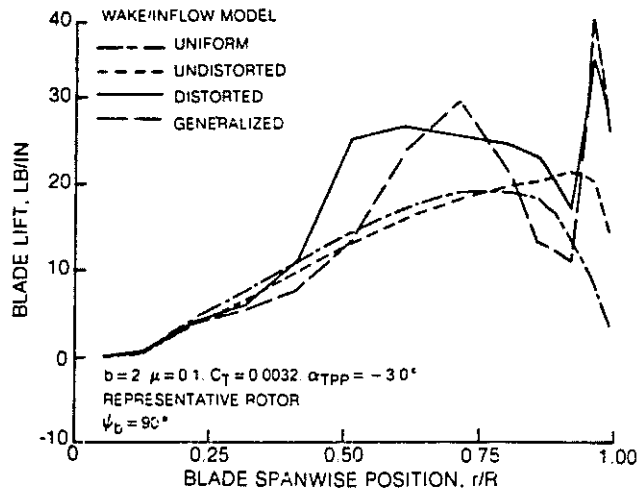

Fig. 30 Predicted Spanwise Lift Distributions for Various Wake/Inflow Models

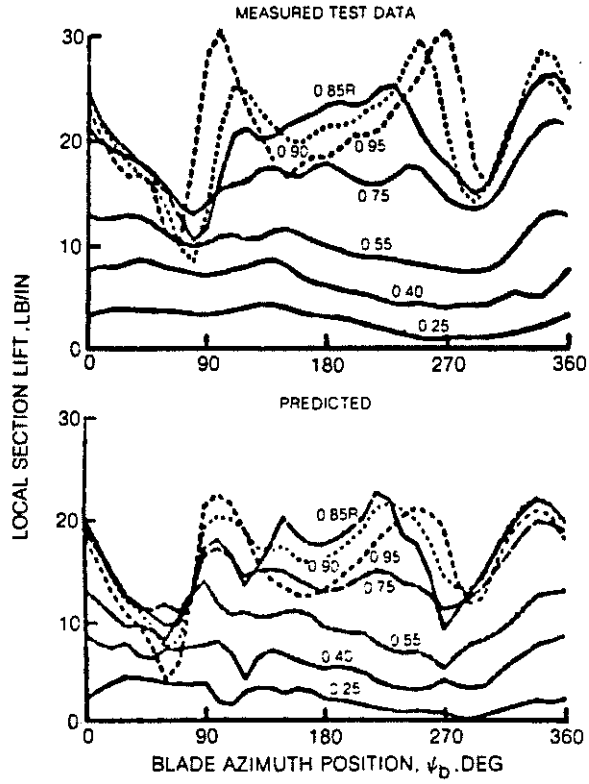

Fig. 31 Measured and Predicted (Distorted Wake) Blade Airloads -- H-34, 48 Kts

spanwise gradients in blade airloads which are not predicted with uniform inflow and undistorted wake analytical models. This is shown in Fig. 29 where the predicted airloads (blade lift distributions) based on the different inflow/wake models are presented for a representative rotor (Refs. 14, 16) in the form of surface contour plots. As indicated, inclusion of tip vortex deformation in the wake model results in increased higher harmonic content in the airload prediction. The outboard advancing side of the rotor typically exhibits the most severe vibratory airload gradients with significant variations also on the outboard retreating side. These impulsive airload characteristics of importance for helicopter vibration have been shown by Hooper (Boeing-Vertol) in Ref. 30 to be surprisingly consistent in test data for different helicopters with substantial differences in size, trim, and number of blades per rotor. A discusion of airloads relevance to helicopter vibration is also contained in Ref. 19. Figure 30 is a plot of the predicted radial distributions of blade loading at the 90 degree azimuth location for this 0.1 advance ratio condition. As can be seen from these results, the features of the distorted wake loading distribution are well represented by the generalized wake loading prediction.

In general, it was found that the influence of wake distortion on blade airloads is directly related to the number and proximity of blade-vortex interactions. The wake influence generally increases with decreasing advance ratio, decreasing nose down tilt of the rotor disk, and increasing number of blades. Increasing thrust coefficient increases the wake deflection angle but also increases the wake distortion toward the rotor. The prediction of tip vortex distortions in close proximity to the blades results in a localized high sensitivity of predicted airloads to small differences in tip vortex geometry. For such conditions, differences in the airload predictions were observed using the generalized and distorted wake models even though the distorted wake geometry appeared to be approximated well by the generalized wake model.

Vibratory airloading is exemplified in the H-34 airload test data shown in Fig. 31, as acquired at 48 kts (0.129 advance ratio) in flight test (Ref. 31). The ability to predict the vibratory airloading characteristics is depicted in Fig. 31 from Refs. 14 and 16, where the results of combining the Sikorsky Generalized Performance Analysis (airloads), the UTRC Rotorcraft Wake Analysis (induced airflow), and the UTRC Wake Geometry Analysis (distorted wake) are presented for the H-34, 48 kt condition. The wake distortions and related airload influence are most complex at low advance ratios, where the difficulty of accurate wake geometry and airloads prediction is compounded by the larger number of close blade-vortex passages and by blade-vortex impingement due to the movement of the tip vortices above and then down through the rotor disk. The prediction of tip vortex distortions, which are in close proximity to the blades at localized regions of the rotor, results in a high sensitivity of predicted air loads to small differences in tip vortex geometry and the theoretical blade-vortex aerodynamic interaction model used. This sensitivity is demonstrated in Refs. 14 and 16. For example, the airload predictions in Fig. 31 resulted from the use of an expanded vortex core model to simulate vortex bursting near close blade passages. Both higher and lower amplitudes of vibratory airloading on the advancing and retreating sides were predicted with other vortex core models and small variations in wake geometry (blade-vortex spacing). Although the need for

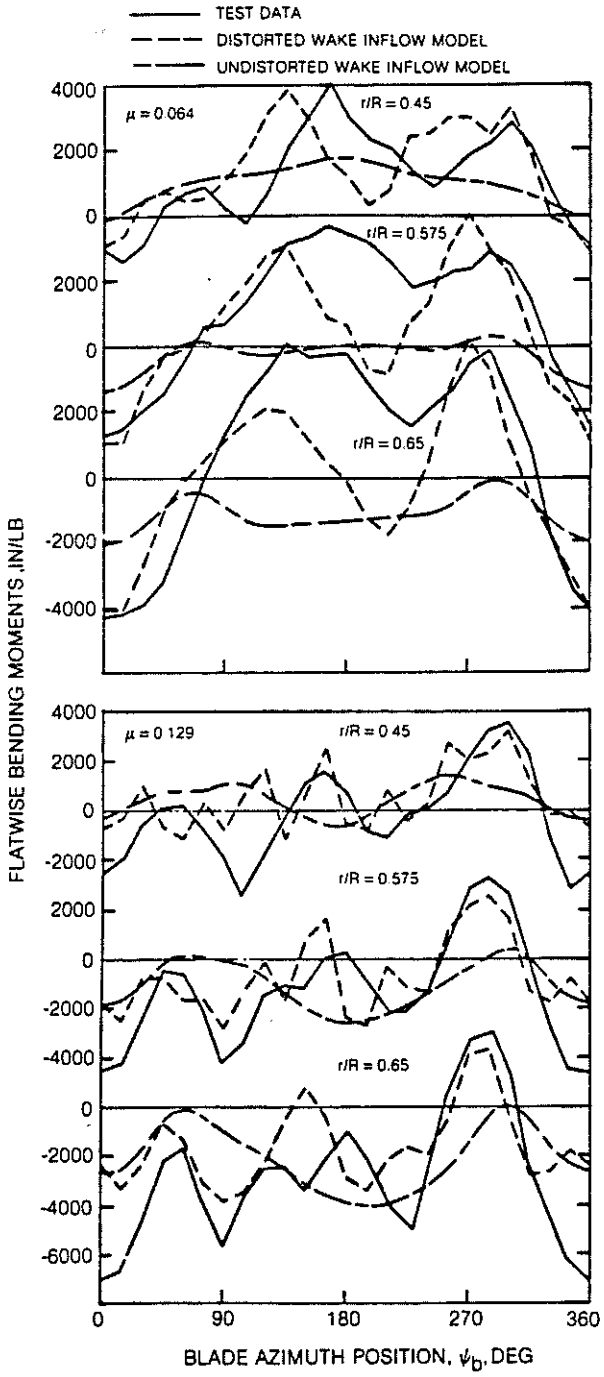

Fig. 32 Comparison of Measured and Predicted H-34 Bending Moments for Advance Ratios 0.064 and 0.129

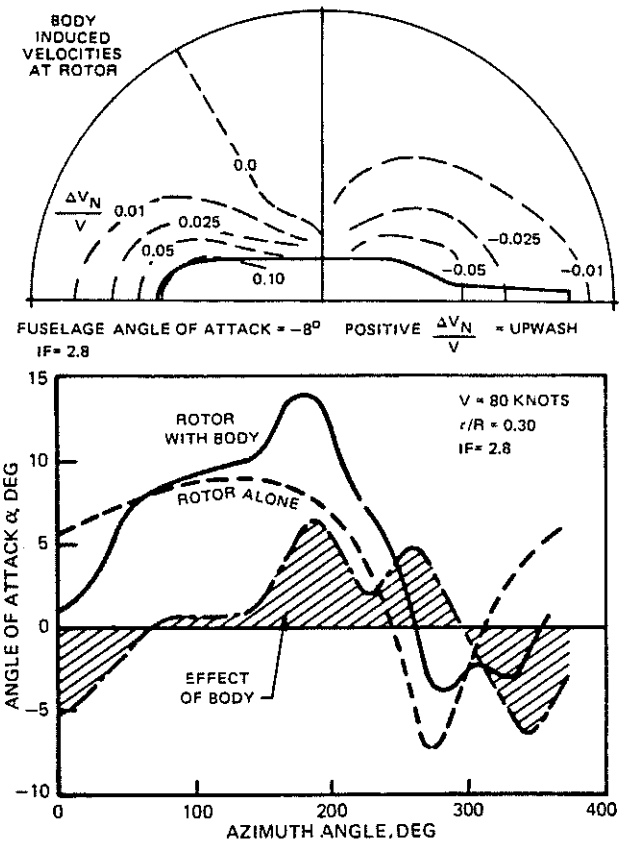

Fig. 33 Predicted Fuselage Induced Velocities at Rotor Disk and Fuselage Effect on Blade Inboard Angle-of-Attack Variation

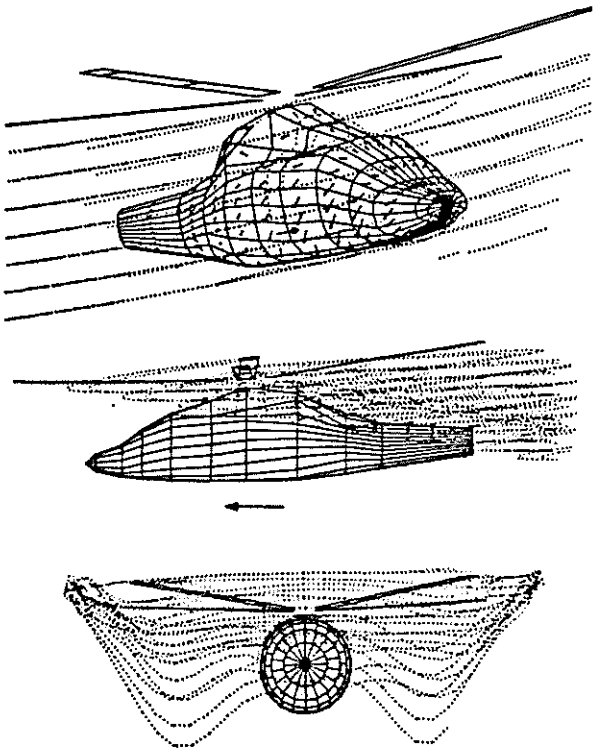

Fig. 34 Wake Modeling for Rotor-Fuselage Aerodynamic Interaction

further analytical refinement is evident, the degree to which the analysis, with a distorted wake model, was able to reproduce the measured airload distributions is encouraging and indicative that, with future emphasis on blade-vortex interaction modeling, wake methodology has the potential to provide a useful predictive tool for vibratory airloads.

Accurate blade airload prediction is required for the prediction of blade bending moments and related blade stresses. To predict the H-34 blade flatwise bending moments for comparison with test data, the Sikorsky Y200 Aeroelastic Rotor Analysis was used with the UTRC Rotorcraft Wake Analysis and the UTRC Wake Geometry Analysis. Overall, the results shown in Fig. 32 indicate that the azimuth variation of the flatwise bending moments is better predicted using the distorted wake inflow model as opposed to the undistorted wake results.

Interactional Airflow and Airloads

Rotor-Fuselage Aerodynamic Interaction

In order to accurately predict helicopter performance and coupled rotor-fuselage vibrations, it is necessary to consider the aerodynamic interaction of the individual components of the helicopter. In Ref. 10 it is shown that the presence of the fuselage distorts the rotor airflow and wake causing two-per-rev as well as other harmonic airload excitations at the rotor. Examples from Ref. 10 of the calculated effect of the airframe presence on the rotor inflow velocities and inner blade angle-of-attack distribution are shown in Fig. 33. Here, the influence of the fuselage on the rotor inflow velocities (ΔV_N) is shown as predicted using the Sikorsky fuselage panel method (WABAT, Ref. 32) for a relatively low rotor configuration (IF = 2.8). (The interference factor, IF, defined in Ref. 10, is representative of the ratio of the fuselage upper surface area to the rotor hub to fuselage distance.) The perturbation of the flow field at the rotor disk produces changes in the blade local angle-of-attack distributions which influence the blade response and airloads. Also in Fig. 33, the angle-of-attack distribution at one radial station is presented as predicted using the UTRC Rotorcraft Wake Analysis coupled with the Sikorsky Generalized Rotor Performance Analysis. In addition to two-per-rev, there is a significant third harmonic content in the increment representing the body induced effect. For low rotor configurations, this should be considered in computations of the vibration spectrum.

The influence of the rotor airflow on fuselage vibratory airloading must also be considered. Experimental results have indicated that the rotor blades and wake can produce significant oscillating fuselage pressures at principally the fundamental blade passage frequency. These pressure pulses have been recognized as a fuselage vibration mechanism, but this mechanism and its effect have not been fully investigated analytically. Methodology is currently being developed at UTRC to approximate the rotor wake deformation due to the fuselage and to calculate the unsteady fuselage pressures. Thus far, provisions have been made for prescribed time variant local deformation of the rotor tip vortices around the fuselage surfaces and the calculation of the airflow and airloads on the panels representing the fuselage surfaces. Wake patterns and flow vectors for sample fuselage shapes and a 0.15 advance ratio condition are shown in Fig. 34.

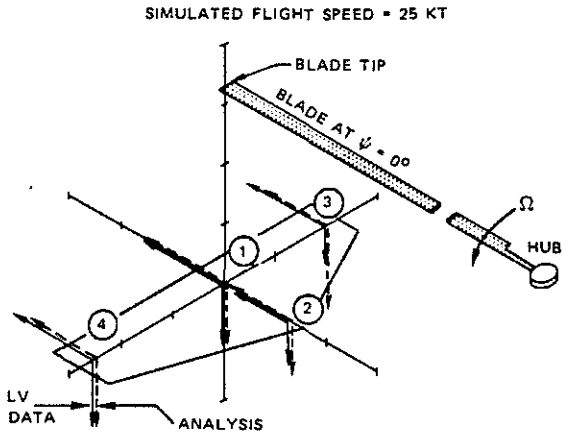

Fig. 35 Predicted Time-Averaged Flow Velocities in Tail Region vs. Laser Velocimeter Data

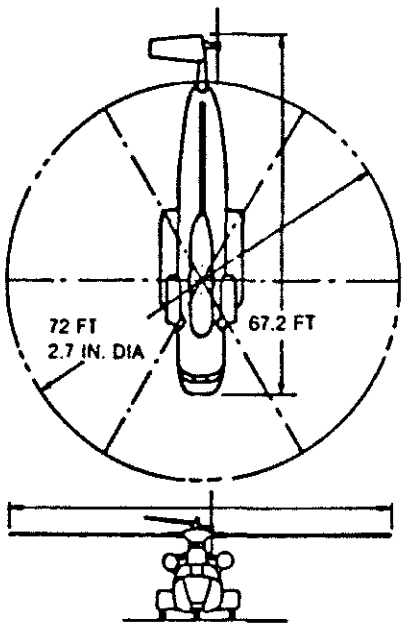

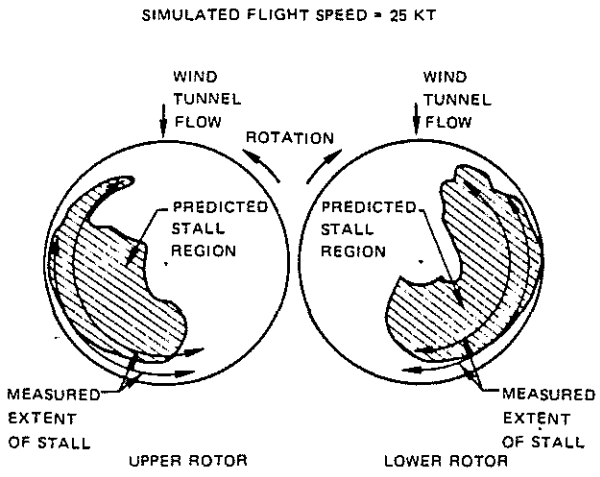

Fig. 37 Coaxial Model Rotor Stall Prediction

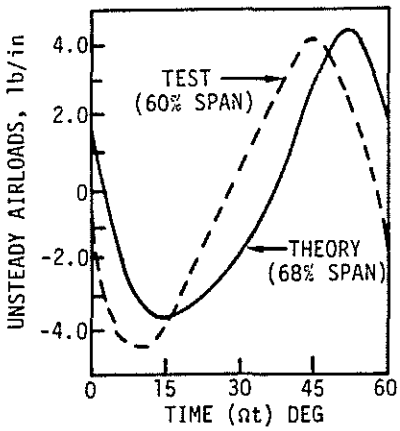

Fig. 36 Comparison of Predicted and Measured Unsteady Airloads Induced by Rotor Wake on CH-53A Horizontal Tail Surface

Rotor-Tail Aerodynamic Interaction

In order to demonstrate the application of the Rotorcraft Wake Analysis for predicting rotor induced interference velocities at a horizontal tail surface of a helicopter, the analysis was used to compare with laser velocimeter data measured in the tail region below a model rotor. Vertical and streamwise flow velocities were measured at four points 0.33R below the rear of a four-bladed, 3.73-ft diameter rotor in a UTRC wind tunnel (tail not present). Time-averaged velocity components, predicted using a calculated distorted wake representation in the Rotorcraft Wake Analysis, are compared with the laser velocimeter measurements in Fig. 35 for a test condition simulating 25 Kt forward speed operation of a full-scale helicopter (Ref. 2). In Fig. 35, one scale division represents a distance of 0.1R and a velocity equal to the momentum value. Good correlation is evident except at one point (point 3), about which significant fluctuations of the wake boundary were predicted.

More recently, a computer program, the Rotor Induced Empennage Vibration Analysis (RIEVA), has been developed at UTRC that predicts the unsteady airloads that are imposed on the empennage surfaces due to aerodynamic interaction with the main rotor wake (Ref. 20). A rotor wake program is used to determine the position and the strength of blade tip vortices that pass near the empennage surfaces. A nonlinear lifting surface analysis is utilized to predict the aerodynamic loads on the empennage surfaces in the presence of these concentrated vortices. The nonlinear analysis was formulated to include pertinent effects such as suction effects of the interacting vortices and the effects of time-variant shed vorticity behind the empennage surfaces. The problem is solved in a stepwise manner (time-domain); that is, a period corresponding to one blade passage is divided into a large number of time intervals and empennage unsteady airloads are computed at each time step. The output of the analysis consists of chordwise and spanwise airload distributions at each time step. These airload distributions are converted into harmonic airloads that can be applied to excite the tail boom in a vibration analysis. The results of a limited correlation study involving the application of the computer program to a full-scale helicopter stabilizer indicate an encouragingly good correlation between the analytical vibratory airload predictions and flight test data. Sample results are shown in Fig. 36 for the 6 per rev airloads of the CH-53A horizontal stabilizer that are induced by the wake of the six-bladed rotor at a high speed condition (159 kts).

Rotor-Rotor Interaction

Although airloads and flow velocity data are not available, an initial evaluation of the Rotorcraft Wake Analysis as applied to coaxial rotor configurations has been conducted by comparing the predicted and measured stall regions of coaxial model rotors. This comparison from Ref. 2 is shown in Fig. 37 for 7-ft diameter coaxial, counter-rotating rotors as operated in a UTRC wind tunnel at a simulated full-scale flight speed of 25 kt. The model rotor was purposely stalled by proper selection of pitch controls and by reducing the rotor tip speed from the nominal full-scale value. The azimuthal extent of stall (blade flow separation) was measured at the 75 and 92 percent radius locations using hot-film gages. (This technique is applied to single rotors in Ref. 21.) Tip vortex coordinates, determined from flow visualization data for both rotors, were used in

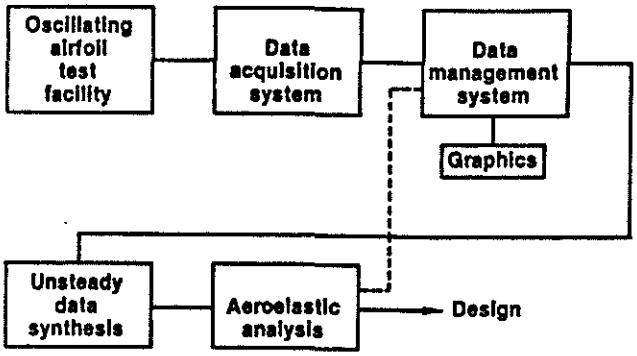

Fig. 38 Empirical Procedure for Unsteady Blade Airloads

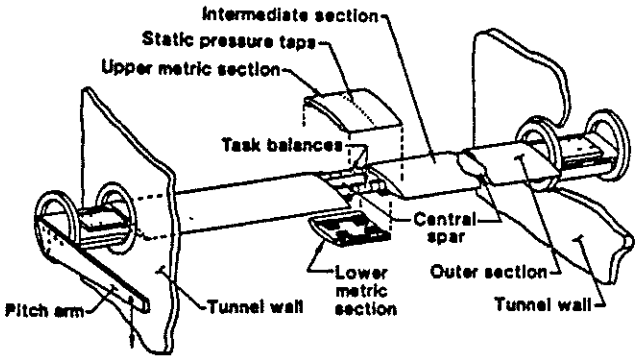

Fig. 39 UTRC Oscillating Tunnel Spanning Wing Assembly (Span = 8 ft)

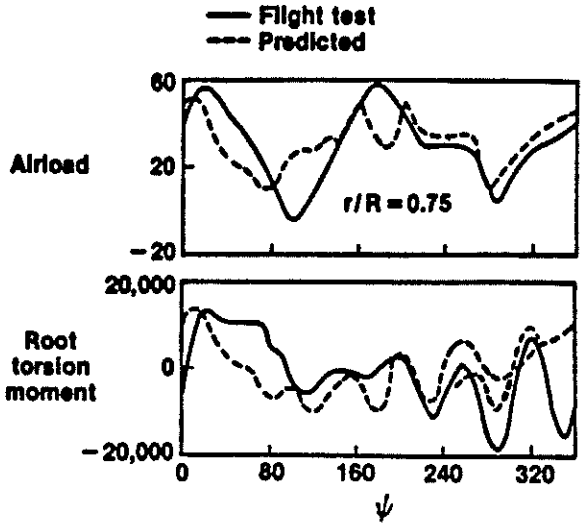

Fig. 41 Comparison of Predicted Blade Airload and Root Torsion Moment With Flight Test Data

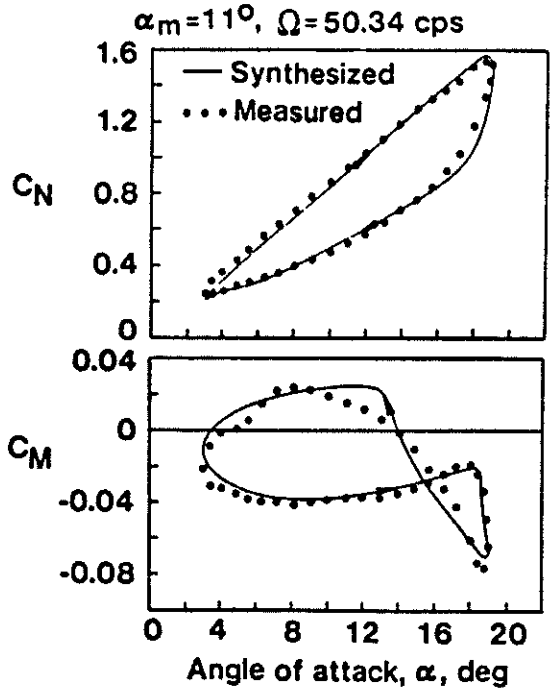

Fig. 40 Comparison of Measured and Synthesized Oscillating Airfoil Data Loops

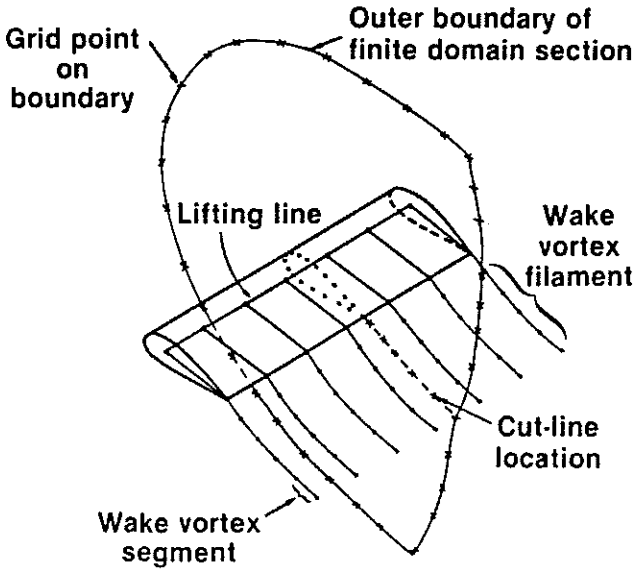

Fig. 42 Finite Domain for Full Potential Flow/Wake Analysis

combination with undistorted inboard wake geometries to prescribe the wake representation in the Rotorcraft Wake Analysis. A local blade section angle of attack of 10 deg was used to define the predicted stall onset and recovery for the operational Reynolds number range of the model rotor. As shown in Fig. 37 the analysis closely predicted the measured extent of stall for both rotors.

Unsteady Airloads and Dynamic Stall

In order to account for the time varying wake circulation shed from the blade and the effects of the formation and streamwise movement of the vortex shed from the airfoil leading edge during dynamic stall, unsteady airfoil data is used in the prediction of rotor blade airloads. The procedure developed at UTRC shown in Fig. 38 is to acquire two-dimensional unsteady lift, drag, and pitching moment data from a tunnel spanning oscillating wing in a wind tunnel (Fig. 39), synthesize the data in terms of rotating blade parameters, and apply the synthesized data in an aeroelastic blade airload analysis. Sample comparisons of measured and synthesized normal force (lift), C_N, and pitching moment, C_M, for an airfoil mean angle and oscillating frequency resulting in dynamic stall is presented in Fig. 40. An example of the capability to predict unsteady blade airloads and root torsion moment for a dynamic stall condition is shown in Fig. 41 in a comparison with CH-53A helicopter flight test data. Sensitivity in the analysis to the flow modeling in the synthesis technique is noted in this figure by the double curve on the retreating side of the rotor. More detailed descriptions of the procedure and applications are presented in Refs. 33, 34, and 35.

Full Potential Flow/Wake Analysis

The Rotorcraft Wake Analysis results presented earlier are based on a lifting-line representation for the blades. In order to provide a more accurate aerodynamic representation of the blades and more properly include chordwise airloading, blade thickness and compressibility effects, a full potential flow analysis has been extended at UTRC for the inviscid solution of the rotor and wake flow field. A NASA three-dimensional full potential analysis (ROT22), described in Refs. 36 and 37, has been recently revised by T. A. Egolf and S. P. Sparks to include the rotor wake influence. The analysis is described and applied to hovering rotor airload prediction in Ref. 38. The NASA analysis, based on an infinite computational domain, was revised to incorporate an inner and outer domain around each blade and match the domain boundary solutions in three dimensions. Blade surface flow and pressure distributions can be computed for subsonic and transonic flow conditions.

Briefly, the method consists of the use of a finite difference scheme to solve the nonlinear near blade flow (inner domain), while the remainder of the flow field (outer domain) is computed using a discrete vortex representation of the wake. A type of solution matching is employed for the resulting inner and outer domain problem. Although the solution is based on the full potential equation, details of the wake distortion are modeled using prescribed wake methods. This allows for the description of the wake to be as complex (or as simple) as desired while maintaining the relatively low cost full potential method for the detailed blade airloads.

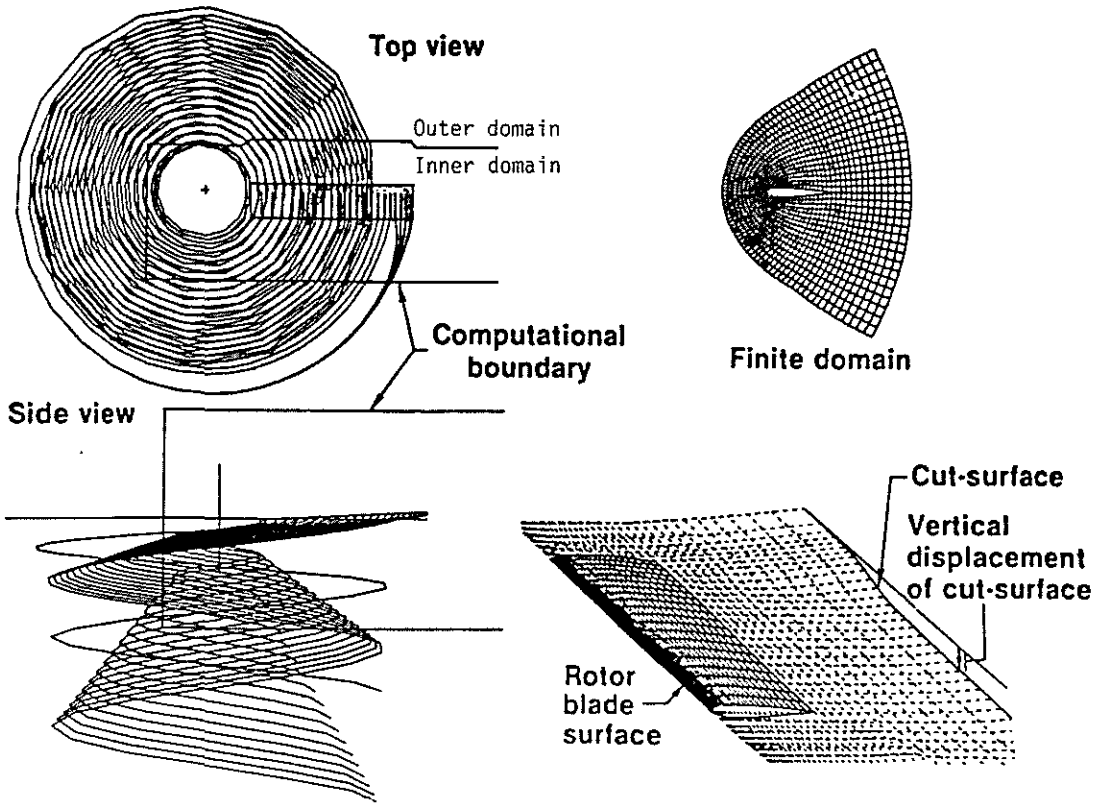

Fig. 43 Schematics of Computational Domain Boundary and Wake Representation

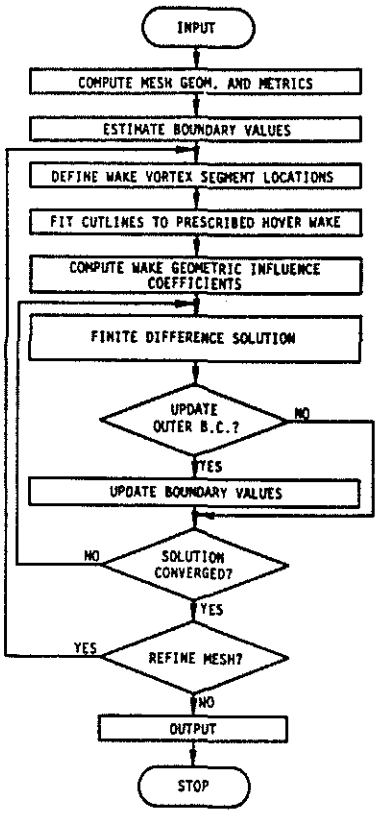

Fig. 44 Solution Procedure for Full Potential Flow/Wake Analysis

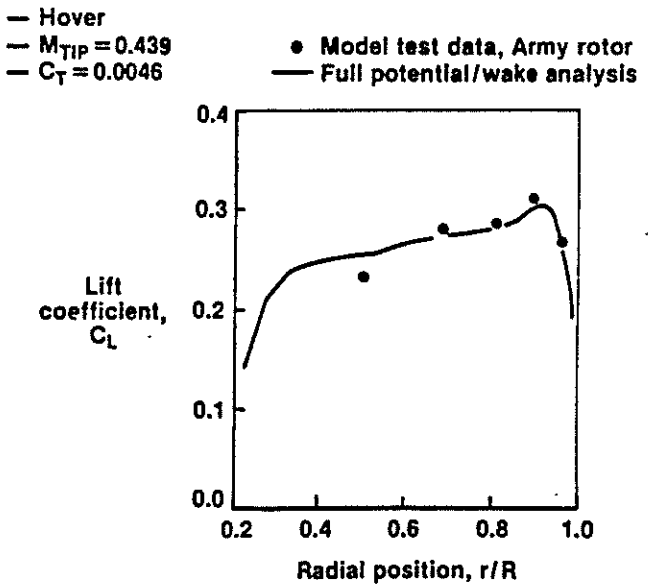

Fig. 45 Comparison of Predicted and Measured Spanwise Lift Distribution

The domain boundary is shown schematically in Fig. 42. To supply the full potential solution with adequate boundary conditions at the domain surface, the segmented lifting line and wake vortex filament representation shown in Fig. 42 is used. The finite inner domain and its computational boundary is shown in Fig. 43 with the hovering blade wake model represented by vortex filaments. The cut-surface (Fig. 43) that represents the blade wake in the inner domain for the full potential solution is adapted to the prescribed wake surface such as that determined from the generalized wake geometry described earlier. An embedded vortex technique has recently been developed to accommodate in the full potential solution the blade-vortex interaction for finite length vortex elements near the blade in the inner domain. The solution procedure for the full potential flow/wake analysis is shown in Fig. 44.

The method of including the wake influence differs from the approach used in the Transonic Small Disturbance method of Ref. 39 which uses an angle-of-attack superposition technique in which the local geometric angle-of-attack is adjusted by an induced angle obtained from a blade wake model.

The analysis has been applied to compare with hover data from model rotors (Ref. 38). A comparison of predicted and measured spanwise lift distributions are presented for an Army rotor (Ref. 40) in Fig. 45. Comparison of chordwise pressure distributions at several spanwise locations are presented in Fig. 46 for subsonic operation. The influence on the chordwise pressure correlation near the blade tip of increasing the tip Mach number to transonic conditions is shown in Fig. 47. The formation of a shock is evident at this location as the blade progresses from low to high tip Mach number. From the increasing upper surface pressure gradient with Mach number in Fig. 47, it is shown that the shock formation feature is predicted by the analysis. This shock is evident in the predicted upper surface isobars shown in Fig. 48.

The concepts involving the inclusion of the influence of the wake using an inner/outer solution domain are not limited to the quasi-steady full potential formulation. The method can be adapted to time-dependent rotor problems and more sophisticated numerical models such as Euler and Navier-Stokes analyses. This method of solution has the advantage of reduced volume for the nonlinear inner domain solution (finite difference methods) while treating the global influence of the complex rotor wake with a method based on prescribed wake models. The computational cost to obtain the complete solution is thus reduced as compared with an infinite domain solution approach.

Several applications have been completed which illustrate the predictive capabilities of the method. The method has recently been extended to forward flight, and forward flight applications and comparisons with test data are presented in Ref. 41.

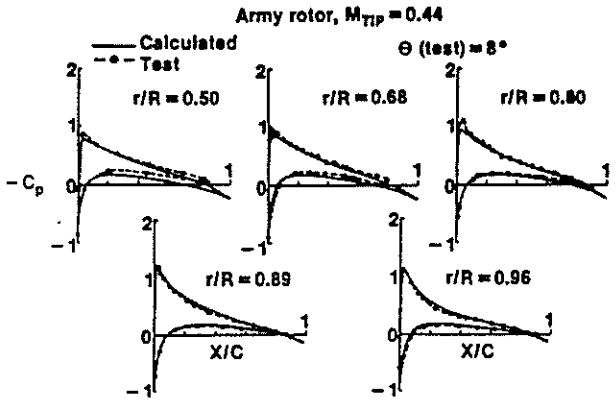

Fig. 46 Comparison of Predicted and Measured Chordwise Pressure Distributions at Several Spanwise Locations

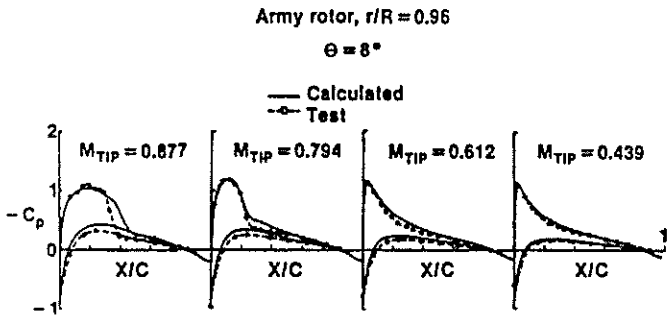

Fig. 47 Comparison of Predicted and Measured Chordwise Pressure Distributions Near Blade Tip for Varying Tip Mach Number

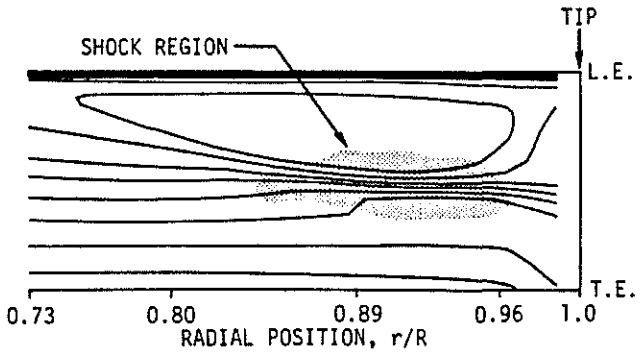

Fig. 48 Predicted Upper Surface Pressure Isobars, $\theta = 8°$, $M_T = 0.877$.

Concluding Remarks

The prediction of helicopter airloads has continued to be a difficult goal due to the compounded complexity of the blade surface aerodynamics, the rotor wake structure and the related flow field. Although the need for further analytical refinement for consistently accurate airflow and airload predictions is evident, the degree to which current analyses reproduce available measured data is "encouraging." The requirement for accurate wake modeling has been demonstrated. The close proximity of tip vortices to the blades at local regions of the rotor results in a high sensitivity of predicted airloads to small differences in tip vortex geometry. This sensitivity demonstrates that fundamental research on blade-vortex interaction and wake structure should continue. Methodology remains to be extended to accurately account for advanced blade design features such as tip shape. Also, the current analyses provide the framework for the computation of helicopter interactional aerodynamics of the various helicopter components, but this is an area that requires continued attention.

More extensive experimental data are required to provide more rigorous validations of methodology. Tests should include a reliable and comprehensive set of performance, airloads and airflow measurements, and the visualization and measurement of the wake structure. Such a test will be conducted by UTRC and Sikorsky in 1986-1987 when extensive measurements of rotor performance, blade airloads, (180 pressure transducers), blade surface flow condition (hot-films), flow velocities (laser velocimeter), and wake geometry (flow visualization) are acquired for hovering model rotors with two advanced tip designs.

With the advent of advanced supercomputers and the rapid progress being made in computational aerodynamics, considerable technology advances for helicopter airload prediction are forseeable in the near future. For example, inclusion of the rotor wake influence in higher level computational aerodynamics methods (unsteady, Euler, and eventually Navier-Stokes analyses), by use of techniques such as that described herein, should be feasible. Also the use of Navier Stokes methods to guide and eventually replace the current empirical approaches involving viscous effects, such as the approach mentioned herein for synthesizing unsteady airfoil characteristics, should provide considerable advancement to rotor airloads technology.

Acknowledgments

The author would like to acknowledge the contributions and support provided by his co-workers and co-authors at UTRC and Sikorsky Aircraft over the past twenty-six years for the many research activities reviewed in this paper. Especially acknowledged is the collaborative support provided by T. Alan Egolf for the past twelve years in wake/airloads methodology development and assessment which has led to his current development of the full potential flow/wake analysis with S. Patrick Sparks and the rotor-fuselage interaction analysis with Peter F. Lorber. The cooperation of Thomas S. Sheehy and Robert M. Moffitt of Sikorsky Aircraft in many related activities is also acknowledged. In addition to UTRC support, funding for the work described herein has been provided by NASA, the Dept. of the Army, and Sikorsky Aircraft.

REFERENCES

1. A. J. Landgrebe, T. A. Egolf — Rotorcraft Wake Analysis for the Prediction of Induced Velocities. USAAMRDL TR-75-45, Jan 1976. (Available from DTIC as AD A021 202.)

2. A. J. Landgrebe, T. A. Egolf — Prediction of Helicopter Induced Flow Velocities Using the Rotorcraft Wake Analysis. Proceedings of the 32nd Annual Forum of the American Helicopter Society, May 1976.

3. A. J. Landgrebe — An Analytical Method for Predicting Rotor Wake Geometry. Journal of the American Helicopter Society, Vol. 14, No. 4, October 1969.

4. A. J. Landgrebe — An Analytical and Experimental Investigation of Helicopter Rotor Hover Performance and Wake Geometry Characteristics. USAAMRDL TR-71-24, U.S. Army, June 1971. (Available from DTIC as AD 728 835.)

5. A. J. Landgrebe — The Wake Geometry of a Hovering Helicopter Rotor and Its Influence on Rotor Performance. Journal of the American Helicopter Society, Vol. 17, No. 4, October 1972. (Also, Proceedings of the 28th Annual National Forum of the American Helicopter Society, May 1972.)

6. D. S. Jenney, J. R. Olson, A. J. Landgrebe — A Reassessment of Rotor Hovering Performance Prediction Methods. Journal of the American Helicopter Society, Vol. 13, No. 2, April 1968 (Also, Proceedings of the 23rd Annual Forum of the American Helicopter Society, May 1967.)

7. E. D. Bellinger — Experimental Effects of Blade Section Camber and Planform Taper on Rotor Hover Performance. USAAMRDL Technical Report 72-4, USAAMRDL, Eustis Directorate, Fort Eustis, VA., March 1972.

8. A. J. Landgrebe, E. D. Bellinger — Experimental Investigation of Model Variable-Geometry and Ogee Tip Rotors. NASA CR-2275, Feb. 1974. (Summarized in paper with same title, Proceedings of the 29th Annual Forum of the American Helicopter Society, May 1973.)

9. D. R. Clark, A. J. Landgrebe — Wake and Boundary Layer Effects in Helicopter Rotor Aerodynamics. AIAA Paper No. 71-581, Presented at the AIAA 4th Fluid and Plasma Dynamics Conference, June 1971.

10. A. J. Landgrebe, R. C. Moffitt, D. R. Clark — Aerodynamic Technology for Advanced Rotorcraft. Journal of the American Helicopter Society, Vol. 22, Nos. 2, 3, April and July 1977 Parts I (pp. 21-27) and II. (Also, Proceedings of Symposium on Rotor Technology, American Helicopter Society, August 1976.)

11. A. J. Landgrebe, T. A. Egolf — Prediction of Rotor Wake Induced Flow Velocities Along the Rocket Trajectories of an Army AH-1G Helicopter. Picatinny Arsenal Technical Report 4797, U.S. Army Picatinny Arsenal, Dover, N.J., March 1975. (Available from DTIC as A007 878.)

12. A. J. Landgrebe, R. B. Taylor, T. A. Egolf, J. C. Bennett — Helicopter Airflow and Wake Characteristics for Low Speed and Hovering Flight from Rocket Interference Investigations. Proceedings of the 37th Annual Forum, American Helicopter Society May 1981, pp. 51-65. (Also, Journal of the American Helicopter Society, Vol. 27, No. 4, October 1982.)

13. A. J. Landgrebe, E. D. Bellinger — An Investigation of the Quantitative Applicability of Model Helicopter Rotor Wake Patterns Obtained from a Water Tunnel. USAAMRDL TR-71-69, December 1971. (Available from DTIC as AD 739 946.)

14. T. A. Egolf, A. J. Landgrebe — Helicopter Rotor Wake Geometry and Its Influence in Forward Flight. Vol. I - Generalized Wake Geometry and Wake Effect on Rotor Airloads and Performance, NASA CR-3726, Oct. 1983.

15. T. A. Egolf, A. J. Landgrebe — Helicopter Rotor Wake Geometry and Its Influence in Forward Flight. Vol. II - Wake Geometry Charts, NASA CR 3727, Oct. 1983.

16. T. A. Egolf, A. J. Landgrebe — Generalized Wake Geometry for a Helicopter Rotor in Forward Flight and Effect of Wake Deformation on Airloads. Proceedings of the 40th Annual Forum of the American Helicopter Society, May 1984.

17. A. J. Landgrebe, B. V. Johnson — Measurement of Model Helicopter Rotor Flow Velocities With a Laser Doppler Velocimeter. Journal of the American Helicopter Society, Vol. 19, No. 3, July 1974, p. 39.

18. A. J. Landgrebe, M. C. Cheney — Rotor Wakes - Key to Performance Prediction . Presented at the Symposium on Status of Testing and Modeling Techniques for V/STOL Aircraft, Mideast Region of the American Helicopter Society, Oct. 1972; (Also, Aerodynamics of Rotary Wing. AGARD CP-111, Feb. 1973, pp. 1-1 to 1-9.)

19. A. J. Landgrebe, M. W. Davis — Analysis of Potential Helicopter Vibration Reduction Concepts. Proceedings of the American Helicopter Society, Ames Research Center 2nd Decennial Specialists' Meeting on Rotorcraft Dynamics, Nov. 1984.

20. S. T. Gangwani — Determination of Rotor Wake Induced Empennage Airloads. Proceedings of the American Helicopter Society National Specialists' Meeting on Helicopter Vibration, Nov. 1981.

21. A. J. Landgrebe, E. D. Bellinger — A Systematic Study of Helicopter Rotor Stall Using Model Rotors. 30th Annual National Forum of the American Helicopter Society, May 1974.

22. T. A. Egolf, S. P. Sparks — Hovering Rotor Airload Prediction Using a Full Potential Flow Analysis with Realistic Wake Geometry. Proceedings of the 41st Annual Forum of the American Helicopter Society, May 1985.

23. T. A. Egolf, A. J. Landgrebe — A Prescribed Wake Rotor Inflow and Flow Field Prediction Analysis - User's Manual and Technical Approach. NASA CR-165894, June 1982.

24. L. J. Bain, A. J. Landgrebe — Investigation of Compound Helicopter Aerodynamic Interference Effects. USAAVLABS Technical Report 67-44, USAAVLABS (now USAAMRDL), Fort Eustis, Va., Nov. 1967.

25. A. Gessow — An Assessment of Current Helicopter Theory in Terms of Early Developments. Fifth Nikolsky Lecture, 41st Annual Forum of the American Helicopter Society, May 1985.

26. J. J. Phillippe, P. Roesch, A. M. Dequin, A. Cler — A Survey of Recent Advances in Helicopter Aerodynamics. AGARD Lecture Series No. 139 on Helicopter Aeromechanics, May 1985.

27. R. M. Moffitt, T. W. Sheehy — Prediction of Helicopter Rotor Performance in Vertical Climb and Sideward Flight. Proceedings of the 33rd Annual Forum of the American Helicopter Society, May 1979.

28. D. W. Boatwright — Measurements of Velocity Components in the Wake of a Full-Scale Helicopter Rotor in Hover. USAAMRDL Technical Report 72-33, Eustis Directorate, USAAMRDL, Fort Eustis, Va., Aug. 1972.

29. J. C. Biggers, K. L. Orloff — Laser Velocimeter Measurements of the Helicopter Rotor-Induced Flow Field. Journal of the American Helicopter Society. Vol. 20, No. 1, Jan. 1975.

30. E. W. Hooper — The Vibratory Airloading of Helicopter Rotors. VERTICA, Vol. 8, NO. 2, 1984. (Also, Proceedings of the Ninth European Rotorcraft Forum, Stresa, Italy, Sept. 1983.)

31. J. Scheiman — A Tabulation of Helicopter Rotor-Blade Differential Pressures, Stresses, and Motions as Measured in Flight. NASA TM X952, March 1964.

32. T. W. Sheehy — A Simplified Approach to Generalized Helicopter Configuration Modeling and the Prediction of Fuselage Surface Pressures. Journal of the American Helicopter Society, Vol. 21, No. 1, Jan. 1976.

33. A. O. St. Hilaire, F. O. Carta, M. R. Fink, W. D. Jepson — The Influence of Sweep on the Aerodynamic Loading on an Oscillating NACA 0012 Airfoil. Vol. I - Technical Report, NASA CR-3092, 1979.

34. S. T. Gangwani — Synthesized Airfoil Data Method for Prediction of Dynamic Stall and Unsteady Airloads. NASA CR 3672, Feb. 1983.

35. S. T. Gangwani — Synthesized Airfoil Data Method for Prediction of Dynamic Stall and Unsteady Airloads. Proceedings of the 39th Annual Forum of the American Helicopter Society, May 1983.

36. R. Arieli, M. E. Tauber — Analysis of the Quasi-Steady Flow About an Isolated Lifting Helicopter Rotor Blade. Joint Institute for Aeronautics and Astronautics TR-24, August 1979.

37. M. E. Tauber, R. M. Hicks — Computerized Three-Dimensional Aerodynamic Design of a Lifting Rotor Blade. Proceedings of the 36th Annual Forum of the American Helicopter Society, May 1980.

38. T. A. Egolf, S. P. Sparks — Hovering Rotor Airload Prediction Using a Full Potential Flow Analysis with Realistic Wake Geometry. Proceedings of the 41st Annual Forum of the American Helicopter Society, May 1985.

39. F. X. Caradonna, C. Tung, A. Desopper — Finite Difference Modeling of Rotor Flows Including Wake Effects. Journal of the American Helicopter Society, April 1984.

40. F. X. Caradonna, C. Tung — Experimental and Analytical Studies of a Model Helicopter Rotor in Hover. NASA TM 81232 (or USAAVRADCOM TR-81-A-23), Sept. 1981.

41. T. A. Egolf, S. P. Sparks — A Full Potential Rotor Analysis With Wake Influence Using an Inner-Outer Domain Technique. Proceedings of the 42nd Annual Forum of the American Helicopter Society, June 1986.